

**Holocene climate variability of the western Mediterranean:  
surface water dynamics inferred from calcareous plankton  
assemblages**

Journal:	<i>The Holocene</i>
Manuscript ID	HOL-19-0114.R1
Manuscript Type:	Paper
Date Submitted by the Author:	30-Oct-2019
Complete List of Authors:	Bazzicalupo, Pietro; Università degli Studi di Bari, Dipartimento di Scienze della Terra e Geoambientali Maiorano, Patrizia; Università degli Studi di Bari, Dipartimento di Scienze della Terra e Geoambientali Girone, Angela; Università degli Studi di Bari, Dipartimento di Scienze della Terra e Geoambientali Marino, Maria; Università degli Studi di Bari, Dipartimento di Scienze della Terra e Geoambientali Combourieu-Nebout, Nathalie; Museum National d'Histoire Naturelle, Homme, Nature et Sociétés Pelosi, Nicola; Istituto di Scienze Marine (ISMAR) - Consiglio Nazionale delle Ricerche, Salgueiro, Emilia; Instituto Português do Mar e da Atmosfera; Universidade do Algarve, Centre of Marine Sciences Incarbona, Alessandro; Università degli Studi di Palermo, Dipartimento di Scienze della Terra e del Mare
Keywords:	Coccolithophores, Foraminifera, Alboran Sea, Holocene, Paleoclimate, Paleoproductivity, Millennial-centennial scale climate variability
Abstract:	A high resolution study (centennial-scale) has been performed on the calcareous plankton assemblage of the Holocene portion of the Ocean Drilling Program Site 976 (Alboran Sea) with the aim to identify main changes in surface water dynamic. The dataset also provided a Seasonal foraminiferal Sea Surface Water Temperatures (SSTs), estimated using the modern analog technique SIMMAX 28, and it was compared with available geochemical and pollen data at the site. Three main climate shifts were identified: I) The increase in abundance of <i>Syracosphaera</i> spp. and <i>Turborotalita quinqueloba</i> marks the early Holocene humid phase, during maximum summer insolation and enhanced river runoff. It is concomitant with the expansion of <i>Quercus</i> , supporting high humidity on land. It ends at 8.2 ka, registering a sudden temperature and humidity reduction; II) The rise in the abundances of <i>Florisphaera profunda</i> and <i>Globorotalia inflata</i> , at ca. 8 ka, indicates the development of the modern geostrophic front, gyre circulation and of a deep nutricline following the sea-level rise; III) The increase of small <i>Gephyrocapsa</i> and <i>Globigerina bulloides</i> at 5.3 ka, suggests enhanced nutrient availability in surface waters, related to more persistent wind-

1  
2  
3  
4  
5  
6  
7  
8  
9  
10  
11  
12  
13  
14  
15  
16  
17  
18  
19  
20  
21  
22  
23  
24  
25  
26  
27  
28  
29  
30  
31  
32  
33  
34  
35  
36  
37  
38  
39  
40  
41  
42  
43  
44  
45  
46  
47  
48  
49  
50  
51  
52  
53  
54  
55  
56  
57  
58  
59  
60

	<p>induced upwelling conditions. Relatively higher winter SST in the last 3.5 kyr favored the increase of <i>Trilobatus sacculifer</i>, likely connected to more stable surface water conditions. Over the main trends, a short term cyclicity is registered in coccolithophore productivity during the last 8 kyr. Short periods of increased productivity are in phase with Atlantic waters inflow, and more arid intervals on land. This cyclicity has been related with periods of positive North Atlantic Oscillation (NAO) circulations. Spectral analysis on coccolithophore productivity confirms the occurrence of millennial-scale cyclicity suggesting an external (i.e. solar) and an internal (i.e. atmospheric/oceanic) forcing.</p>

SCHOLARONE™  
Manuscripts

1  
2  
3 1 **Holocene climate variability of the western Mediterranean: surface water dynamics inferred**  
4 **from calcareous plankton assemblages**  
5 2  
6 3

8 4 Pietro Bazzicalupo<sup>1</sup>, Patrizia Maiorano<sup>1</sup>, Angela Girone<sup>1</sup>, Maria Marino<sup>1</sup>, Nathalie Combourieu-  
9 Nebout<sup>2</sup>, Nicola Pelosi<sup>3</sup>, Emília Salgueiro<sup>4,5</sup>, Alessandro Incarbona<sup>6</sup>

12 6  
13 7 1 Dipartimento di Scienze della Terra e Geoambientali, Università degli Studi di Bari Aldo Moro, via E.  
14 Orabona 4, 70125, Bari, Italy

16 9 2 French National Centre for Scientific Research UMR 7194 - Histoire Naturelle de l'Homme Préhistorique,  
17 Paris, France

19 10 3 Istituto di Scienze Marine (ISMAR) - Consiglio Nazionale delle Ricerche, Calata Porta di Massa, 80133-  
20 Napoli, Italy

22 12 4 Div. Geologia e Georecursos Marinhos, Instituto Português do Mar e da Atmosfera (IPMA), Lisbon, 1749-  
23 077, Portugal

25 14 5 Centre of Marine Sciences, Universidade do Algarve, Faro, 8005-139, Portugal.

27 16 6 Università di Palermo, Dipartimento di Scienze della Terra e del Mare, Via Archirafi 22, 90134 Palermo,  
28 Italy

31 18  
32  
33 19 **Keywords**

34 20 Coccolithophores, Foraminifera, Alboran Sea, Holocene, Paleoclimate, Paleoproductivity,  
35 Millennial-centennial scale climate variability  
36 21

38 22  
39 23 **Abstract**

41 24 A high resolution study (centennial-scale) has been performed on the calcareous plankton assemblage  
42 of the Holocene portion of the Ocean Drilling Program Site 976 (Alboran Sea) with the aim to identify  
43 25 main changes in surface water dynamic. The dataset also provided a Seasonal foraminiferal Sea  
44 26 Surface Water Temperatures (SSTs), estimated using the modern analog technique SIMMAX 28, and  
45 27 it was compared with available geochemical and pollen data at the site.

48 28 Three main climate shifts were identified: I) The increase in abundance of *Syracosphaera* spp. and  
49 29 *Turborotalita quinqueloba* marks the early Holocene humid phase, during maximum summer  
50 30 insolation and enhanced river runoff. It is concomitant with the expansion of *Quercus*, supporting  
51 31 high humidity on land. It ends at 8.2 ka, registering a sudden temperature and humidity reduction; II)  
52 32 The rise in the abundances of *Florisphaera profunda* and *Globorotalia inflata*, at ca. 8 ka, indicates  
53 33 the development of the modern geostrophic front, gyre circulation and of a deep nutricline following  
54 34 the sea-level rise; III) The increase of small *Gephyrocapsa* and *Globigerina bulloides* at 5.3 ka,  
55 35  
56  
57  
58  
59  
60

1  
2  
3 36 suggests enhanced nutrient availability in surface waters, related to more persistent wind-induced  
4  
5 37 upwelling conditions. Relatively higher winter SST in the last 3.5 kyr favored the increase of  
6  
7 38 *Trilobatus sacculifer*, likely connected to more stable surface water conditions. Over the main trends,  
8  
9 39 a short term cyclicality is registered in coccolithophore productivity during the last 8 kyr. Short periods  
10 40 of increased productivity are in phase with Atlantic waters inflow, and more arid intervals on land.  
11  
12 41 This cyclicality has been related with periods of positive North Atlantic Oscillation (NAO) circulations.  
13  
14 42 Spectral analysis on coccolithophore productivity confirms the occurrence of millennial-scale  
15 43 cyclicality suggesting an external (i.e. solar) and an internal (i.e. atmospheric/oceanic) forcing.  
16  
17 44

## 18 45 **Introduction**

20 46 An increasing number of climate records reveals that the Holocene has experienced a pervasive  
21  
22 47 millennial- and centennial-scale climate variability (e.g. Jalut et al., 2009; Magny et al., 2013;  
23  
24 48 Mayewski et al., 2004; Walker et al., 2012; Wanner et al., 2015), well-documented in both the North  
25  
26 49 Atlantic (e.g. Bond et al., 2001; Repschläger et al., 2017; Thornalley et al., 2009) and western  
27  
28 50 Mediterranean (e.g. Ausín et al., 2015a; Cacho et al., 2001; Català et al., 2018; Frigola et al., 2007;  
29  
30 51 Jalali et al., 2017, 2016; Nieto-Moreno et al., 2015; Rodrigo-Gámiz et al., 2011). The western  
31  
32 52 Mediterranean Sea is in fact extremely sensitive to the changes experienced in the North Atlantic and  
33  
34 53 is an ideal location for high-frequency climatic investigations, because water mass properties changes  
35  
36 54 and oceanographic and atmospheric circulation oscillations are usually amplified (Cacho et al., 1999,  
37  
38 55 2001; Català et al., 2018; Frigola et al., 2007, 2008; Jalali et al., 2016; Moreno et al., 2002; Nieto-  
39  
40 56 Moreno et al., 2015; Sierro et al., 2005; Toucanne et al., 2012). The millennial-scale climate  
41  
42 57 variability in the western Mediterranean is reflected in different water column configurations and  
43  
44 58 oceanographic features (e.g. fronts and eddies) that left a clear signature in the calcareous plankton  
45  
46 59 assemblages (Ausín et al., 2015a; Pérez-Folgado et al., 2003, 2004; Sbaffi et al., 2001). During the  
47  
48 60 Holocene, the Alboran Sea experienced relevant oceanographic perturbations, the most important of  
49  
50 61 which was the instauration of the modern geostrophic front and establishment of gyre anticyclonic  
51  
52 62 circulation dynamics, following sea level rising after the last deglaciation (Ausín et al., 2015b; Català  
53  
54 63 et al., 2018; Colmenero-Hidalgo et al., 2004; Heburn and La Violette, 1990; Rohling et al., 1995;  
55  
56 64 Weaver and Pujol, 1988). This important change also marked the end of the Organic Rich Layer 1  
57  
58 65 (ORL1) deposition in the western Mediterranean (Bárcena et al., 2001; Cacho et al., 2002; Jimenez-  
59  
60 66 Espejo et al., 2007, 2008; Rogerson et al., 2008). Targeting the high frequency oscillations  
61  
62 67 experienced during the Holocene, a growing attention has been focused on the impact of the North  
63  
64 68 Atlantic Oscillation (NAO) atmospheric pattern in the western Mediterranean Sea, in terms of  
65  
66 69 westerlies strength and deep water production, precipitation and river runoff, and coccolithophore

1  
2  
3 70 productivity (Ausín et al., 2015a; Fletcher et al., 2012; Frigola et al., 2007; Jalali et al., 2016; Moreno  
4 71 et al., 2005; Smith et al., 2016; Trigo et al., 2004; Zielhofer et al., 2017). However, only a few studies  
5 72 so far have documented the relationship between coccolithophore productivity and atmospheric  
6 73 variability, like the present NAO index (e.g. Ausín et al., 2015a).

7 74 In this framework we carried out, over the last 12 ka, at the Ocean Drilling Program (ODP) Site 976,  
8 75 an integrated study between coccolithophores and planktonic foraminifera by a centennial-scale  
9 76 resolution, not available so far in the Alboran Sea. The aim was to reconstruct paleoenvironmental  
10 77 fluctuations in the Alboran Sea and to discuss the mechanisms controlling fossil assemblage and  
11 78 productivity variations at different time scales. A planktonic foraminifera-based Sea Surface  
12 79 Temperature (SST) reconstruction is also provided, to have further insights on seasonal and annual  
13 80 temperature variations. In addition, spectral and wavelet analyses of the coccolithophore  
14 81 accumulation rates are performed to identify the different periodicities of coccolithophore  
15 82 productivity fluctuations. The study also benefits from the comparison with additional inorganic and  
16 83 organic geochemical proxies (Jiménez-Amat and Zahn, 2015; Martrat et al., 2014) and pollen data  
17 84 (Combourieu-Nebout et al., 2009) available at the same site, improving the paleoclimate  
18 85 reconstruction through a direct multi-proxy approach.  
19 86

## 20 87 **Area of Study**

### 21 88 *Present hydrographical conditions*

22 89 The ODP Site 976 was recovered off the Spanish coast in the Alboran Sea, the westernmost basin of  
23 90 the Mediterranean Sea, bordering the Atlantic Ocean (Fig. 1). Surrounding lands include the high  
24 91 physiography of the Betic cordillera and Moroccan Rif mountains, that might provide a certain  
25 92 riverine input, although subjected to high seasonality and extreme climatic events (Jimenez-Espejo  
26 93 et al., 2008; Liqueste et al., 2005; Lobo et al., 2006). Surface Atlantic Water (AW) pours inside the  
27 94 Alboran basin through the Strait of Gibraltar, as a constant stream of surface low-salinity waters  
28 95 called the Atlantic Jet (AJ). The latter contributes to the creation of two quasi-permanent meso-scale  
29 96 anticyclonic gyres: the Western Anticyclonic Gyre (WAG) and the Eastern Anticyclonic Gyre (EAG)  
30 97 (Fig. 1) (Heburn and La Violette, 1990; Sarhan et al., 2000). In the area, two mechanisms are known  
31 98 to be relevant for the upwelling dynamic: the southward drifting of the AJ, that would allow the water  
32 99 from below to rise, and the wind stress (Sarhan et al., 2000). The influence of the vertical mixing of  
33 100 AJ and deeper Mediterranean waters, concurrently with the complex bottom topography, forms areas  
34 101 of geostrophic front and quasi-permanent upwelling: the Alboran front and the Almeria-Oran front  
35 102 (Fig.1) (Perkins et al., 1990; Viúdez et al., 1996).  
36  
37  
38  
39  
40  
41  
42  
43  
44  
45  
46  
47  
48  
49  
50  
51  
52  
53  
54  
55  
56  
57  
58  
59  
60

1

2

3 103 The combination of gyres and upwelling fronts results in increased nutrient availability and high  
4 104 productivity waters, among the richest within the rest of the Mediterranean (D'Ortenzio and  
5 105 D'Alcalà, 2009; Garcia-Gorrioz and Carr, 1999). Counteracting the AW inflow, the denser and more  
6 106 saline Mediterranean waters exit the basin through the Mediterranean Outflow Water (MOW), that  
7 107 includes the western Mediterranean Deep Water (WMDW) from the Gulf of Lion and the Levantine  
8 108 Intermediate Water (LIW) from the far East of the Mediterranean basin (Fig. 1) (Millot, 2008; Perkins  
9 109 et al., 1990). Deep water formation is controlled by surface heat loss due to winds blowing from the  
10 110 north and north-west (Font et al., 2007; Mertens and Schott, 1998; Rixen et al., 2005; Smith et al.,  
11 111 2008).

12

13

14

15

16

17

18

19

20

21

22

23

24

25

26

27

28

29

30

31

32

33

34

35

36

37

38

39

40

41

42

43

44

45

46

47

48

49

50

51

52

53

54

55

56

57

58

59

60

### *Present Climate Conditions*

114 The Alboran Sea climate conditions are under the influence of the Azores high pressure cell and its  
115 seasonal latitudinal shift, resulting in mild wet winters and dry hot summers (Lionello, 2012; Moreno  
116 et al., 2012; Rohling et al., 2015; Sumner et al., 2001). At decadal and inter-annual time scales,  
117 atmospheric variability is regulated by the North Atlantic Oscillation (NAO) index, which is  
118 characterized by positive (NAO+) and negative (NAO-) regimes (Hurrell, 1995; Olsen et al., 2012;  
119 Smith et al., 2016; Trigo et al., 2004). During a NAO+ regime, stronger pressure difference between  
120 the Azores High and Icelandic Low atmospheric cells brings storm trajectories to the north,  
121 determining stormier and wetter weather in northwest Europe and dryer winters in southern Europe  
122 and North Africa (Olsen et al., 2012; Smith et al., 2016; Zielhofer et al., 2017). At NAO- regime,  
123 weaker difference between the two pressure cells leads storm tracks to the south, enhancing  
124 precipitations over southern Europe and North Africa (Smith et al., 2016; Wanner et al., 2015). In the  
125 Iberian Peninsula, winter precipitation mode has been related to air masses raised by atmospheric  
126 instabilities and moisture supply from the tropical-subtropical North Atlantic corridor (Gimeno et al.,  
127 2010).

## **Materials and Methods**

### *Core material and available data sets*

131 The ODP Site 976 (Comas et al., 1996) is located about 60 km south of the Iberian Peninsula and  
132 about 110 km East of the Strait of Gibraltar (36°12.3' N, 4°18.7' W) (Fig. 1). The cores were recovered  
133 on the lower part of a very gentle slope, dipping southward of the Spanish margin in the Alboran  
134 Basin, at a depth of 1108 m. The investigated sediments are from Hole C – Core 1H – sections 1-3  
135 (Comas et al., 1996), between 0.07 to 4.03 m below the sea floor. Main lithology is composed of  
136 nanofossil rich clay, with slight to moderate bioturbation and common shell fragments (Comas et

1  
2  
3 137 al., 1996). One Organic Rich Layer (ORL) occurs in the studied interval and is identified on the basis  
4  
5 138 of the maximum accumulation of di- and tri- alkenones of 37 carbons (Martrat et al., 2004, 2014).  
6  
7 139 The age model used in the present study is from Martrat et al. (2014), based on available <sup>14</sup>C calibrated  
8  
9 140 AMS radiocarbon dates (Combourieu-Nebout et al., 2002, 2009). Sampling resolution of calcareous  
10 141 plankton dataset varies between 1 sample every 2 to 6 cm, according to the variable sedimentation  
11  
12 142 rate (20 to 60 cm), thus providing a temporal resolution of one sample every ca. 100 years.

### 13 14 143 15 144 *Calcareous plankton*

16  
17 145 The coccolith assemblages were analyzed in 129 samples. Sample preparation for the coccolith  
18  
19 146 analysis follows the random settling technique by Flores and Sierro (1997). The quantitative analyses  
20  
21 147 were performed using a polarized light microscopy at 1000X magnification. The relative abundance  
22 148 of taxa was estimated counting at least 500 specimens per sample, in variable fields of view.  
23  
24 149 Reworked calcareous nannofossils were estimated separately during this counting. The absolute  
25  
26 150 abundance of taxa is expressed as Nannofossil Accumulation Rate (NAR). The total NAR, used to  
27  
28 151 determine coccolithophore paleoproductivity (Baumann et al., 2004; Steinmetz, 1994), was estimated  
29 152 following Flores and Sierro (1997):

$$30 \quad \text{NAR} = \mathbf{N} * \mathbf{w} * \mathbf{S}$$

31 153  
32  
33 154 where **N** is the number of coccoliths per gram of sediment ( $\text{Ng}^{-1}$ ), **w** is the wet bulk density ( $\text{g}\times\text{cm}^{-3}$ )  
34 155 (shipboard bulk density data, Comas et al., 1996), and **S** is the sedimentation rate ( $\text{cm}\times\text{ky}^{-1}$ ). Wet  
35  
36 156 bulk density is frequently used as a substitute to dry bulk density, in the absence of the latter, to  
37  
38 157 estimate coccolithophore production (Grelaud et al., 2009; Marino et al., 2014; Stolz and Baumann,  
39  
40 158 2010). For taxonomic identification we referred to Young et al. (2003) and Jordan et al. (2004).  
41 159 According to Flores et al. (2000): gephyrocapsids with high angle bridge ( $>50^\circ$ ) and  $>3 \mu\text{m}$  in size  
42  
43 160 are indicated as *Gephyrocapsa oceanica*; gephyrocapsids  $>3 \mu\text{m}$  in size with a low angle bridge ( $<$   
44  
45 161  $25^\circ$ ) are indicated as *Gephyrocapsa muellerae*; small *Gephyrocapsa* includes gephyrocapsids  $< 3\mu\text{m}$   
46 162 in size. Specimens of *Emiliania huxleyi* were differentiated into two main groups following size  
47  
48 163 criteria (Colmenero-Hidalgo et al., 2002): large *E. huxleyi*  $> 4 \mu\text{m}$  and small *E. huxleyi*  $< 4 \mu\text{m}$ . Warm  
49  
50 164 water taxa are grouped according to their ecological preference for tropical-subtropical waters  
51  
52 165 (Baumann et al., 2004; Boeckel and Baumann, 2004; Winter and Siesser, 1994). The group includes:  
53 166 *Calciosolenia* spp., *Discosphaera tubifera*, *Rhabdosphaera stylifera*, *Rhabdosphaera clavigera*,  
54  
55 167 *Umblicosphaera foliosa*, *Umblicosphaera sibogae*, *Umbellosphaera* spp., *Oolithotus* spp.  
56  
57 168 Planktonic foraminifera assemblages were analyzed in 122 samples washed through 63 and 150 $\mu\text{m}$   
58  
59 169 sieves. The residues ( $>150\mu\text{m}$ ) were split, until a representative aliquot containing about 300  
60 170 specimens has been obtained. All specimens were counted in the aliquots and species abundances

1  
2  
3 171 were quantified as percentages on the total number of planktonic foraminifers (relative abundance)  
4  
5 172 and as absolute abundances expressed as planktonic foraminifera Accumulation Rates (pfAR). The  
6  
7 173 pfAR has been calculated following Giraudeau et al. (2001):

$$8 \quad 174 \quad \text{pfAR} = \text{AA} * \mathbf{w} * \mathbf{S}$$

9  
10 175 where **AA** is the number of specimens per gram of dry sediment (nr/g), **w** is the wet bulk density  
11  
12 176 ( $\text{g} \times \text{cm}^{-3}$ ) (shipboard bulk density data, Comas et al., 1996), and **S** is the sedimentation rate ( $\text{cm} \times \text{ky}^{-1}$ ).  
13  
14 177 Sixteen species or species groups were distinguished. *Globigerinoides ruber* includes morphotypes  
15 178 of *G. ruber* white, and *Globigerinoides elongatus* (sensu Aurahs et al., 2011); *Trilobatus sacculifer*  
16  
17 179 includes *Trilobatus trilobus*, *Trilobatus sacculifer* and *Trilobatus quadrilobatus* (sensu André et al.,  
18  
19 180 2012; Hemleben et al., 1989; Spezzaferri et al., 2015). *Globoturborotalita rubescens* includes  
20  
21 181 *Globoturborotalita tenella* because of their similar ecological preference (Capotondi et al., 1999).  
22 182 The taxonomy of *Neogloboquadrina* spp. follows criteria by Darling et al., (2006):  
23  
24 183 *Neogloboquadrina incompta* includes specimens previously referred to *N. pachyderma* (dextral) and  
25  
26 184 intergrades between *N. pachyderma* (dextral) and *N. dutertrei*. *Neogloboquadrina pachyderma* only  
27 185 includes the left coiling specimens.

28  
29 186 According to their ecological preference (Hemleben et al., 1985; Kucera et al., 2005; Pujol and  
30  
31 187 Vergnaud-Grazzini, 1995) and to previous Mediterranean Sea paleoclimatic reconstructions (De Rijk  
32  
33 188 et al., 1999; Rohling et al., 1997), *G. ruber*, *T. sacculifer*, *Hastigerina pelagica*, *G. rubescens*,  
34 189 *Orbulina universa*, *Beella digitata* and *Globigerinella siphonifera* have been grouped as warm water  
35  
36 190 taxa.

### 37 38 191 39 192 *Sea Surface Temperature estimation*

40  
41 193 Planktic foraminifera assemblages were used to reconstruct annual, summer (July to September) and  
42  
43 194 winter (January to March) SST with the modern analog technique non distance-weighted SIMMAX  
44  
45 195 28 and 10 analogs (Pflaumann et al., 1996). Considering that the study site is influenced by Atlantic  
46 196 and Mediterranean ocean circulation, following Schirrmacher et al. (2019), we use the combined  
47  
48 197 North Atlantic core-top database (Kucera et al., 2005; Salgueiro et al., 2010, 2014) and the  
49  
50 198 Mediterranean database (Hayes et al., 2005), and the root mean square error of both annual and  
51  
52 199 seasonal SST reconstructions is about 1.3°C (Schirrmacher et al., 2019).

### 53 200 54 55 201 *Power spectral and wavelet analysis*

56  
57 202 Spectral and wavelet analyses were performed on the total NAR, displaying relevant high frequency  
58  
59 203 oscillations throughout the record. The analysis of the non-stationary (frequency changes along time)  
60 204 and non-linear signals, was performed by applying the Empirical Mode Decomposition algorithm



(EMD) of Huang et al. (1998) in order to decompose multi-component signals into a series of amplitude and frequency modulation (AM-FM) waves, each with slowly varying amplitude and phase. A major advantage of EMD is that the basis functions are derived from the signal itself, hence the analysis is adaptive, in contrast to the traditional methods where the basis functions are fixed as sine and cosine for Fourier transform like methods and the mother wavelet functions for wavelet analysis.

The signal and the Intrinsic Mode Functions (IMF) components are analysed without interpolation, keeping the original evenly sampling intervals, with:

1. "REDFIT", that computes the spectrum of a possibly unevenly sampled time-series, by using the Lomb-Scargle Fourier transform. The spectrum is bias-corrected using spectra computed from simulated AR(1) series and the theoretical AR(1) spectrum (Lomb, 1976; Scargle, 1982; Schulz and Mudelsee, 2002).
2. Foster's (1996) weighted wavelet Z-transform (WWZ). To analyze non-stationary and irregularly sampled signals, we need an extension of the classic wavelet formalism. Foster (1996), who defines the WWZ, developed such extension as a suitable weighted projection method re-orthogonalizing the three basic functions (real and imaginary part of the Morlet wavelet and a constant) by rotating the matrix of their scalar products. Furthermore, he introduces statistical F-tests to distinguish between periodic components and a noisy background signal.

## Results

### *Calcareous nannofossils*

Calcareous nannofossils are generally abundant and well preserved and dissolution phenomena seem not to be significant. Abundances of the most relevant taxa are presented in Fig. 2 and no major discrepancies are observed between relative and absolute trends. The total NAR ranges between  $0.5 \times 10^{11}$  coccoliths  $\times \text{cm}^{-2} \times \text{kyr}^{-1}$  and  $2 \times 10^{11}$  coccoliths  $\times \text{cm}^{-2} \times \text{kyr}^{-1}$ , with an average of  $0.8 \times 10^{11}$  coccoliths  $\times \text{cm}^{-2} \times \text{kyr}^{-1}$  (Fig. 2). A marked abundance peak occurs at about 8.2 ka, and an oscillating pattern is recorded in the last 8 kyr (Fig. 2). Considering the relative abundances of the taxa (%), *E. huxleyi* < 4  $\mu\text{m}$  represents the main taxon, having percentages between 40 and 60% and the highest values between 10 and 8 ka (Fig. 2). Among geophyrocapsids, *G. muelleriae* results to be the most abundant in the lower part of the record, with values reaching 30% of the assemblage, followed by a descending trend (Fig. 2). Small *Gephyrocapsa* show an increase in abundance from 8%, between 10 and 7 ka, to 15% from 5.3 ka upward (Fig. 2). *Gephyrocapsa oceanica*, mainly represented by morphotypes larger than 5  $\mu\text{m}$ , shows abundance fluctuations between 3 and 10% throughout the

1  
2  
3 239 Holocene (Fig. 2). *Florisphaera profunda*, although not a dominant component of the assemblages  
4  
5 240 (with very few isolated peaks greater than 15%), shows a distinct pattern, with very low percentage  
6  
7 241 values up to ~8 ka, that clearly increase upwards in fluctuating abundances (Fig. 2). Among less  
8  
9 242 abundant taxa, *Syracosphaera* spp. (*S. histrica* and *S. pulchra*), having a mean value of 1%, show a  
10 243 distinct increase between 11 and 8 ka, reaching values of about 5% (Fig. 2). The warm water coccolith  
11  
12 244 taxa have very low abundances throughout the succession, with a mean value of 2%; the group shows  
13  
14 245 a gradual increase between 12 and 8 ka, and fluctuating pattern afterwards (Fig. 2). *Helicosphaera*  
15 246 *carteri* and *E. huxleyi* > 4  $\mu\text{m}$  show a similar pattern with abundance values ranging between 10 and  
16  
17 247 15% in the lowest part of the succession (during the Younger Dryas), followed by a clear decreasing  
18  
19 248 trend, with values around 1% (Fig. 2). Other taxa, not showing particular trends or significant  
20  
21 249 fluctuations, are represented by *Coccolithus pelagicus* ssp. *pelagicus*, *Gephyrocapsa caribbeanica*  
22 250 and *Coronosphaera* spp., with percentages not higher than 5%. Subordinate taxa do not exceed the  
23  
24 251 3% of the assemblage and include *Coccolithus pelagicus* ssp. *braarudii*, *Coccolithus pelagicus* ssp.  
25  
26 252 *azorinus*, *Braarudosphaera bigelowii*, *Calcidiscus leptoporus* ssp. small (3–5  $\mu\text{m}$ ), *C. leptoporus* ssp.  
27 253 *leptoporus* (5–8  $\mu\text{m}$ ), *C. leptoporus* ssp. *quadriperforatus* (8–10  $\mu\text{m}$ ), *Ceratolithus* spp.,  
28  
29 254 *Helicosphaera pavementum*, *Helicosphaera hyalina*, *Pontosphaera* spp., *Gladiolithus flabellatus*,  
30  
31 255 *Scyphosphaera* spp. and *Umbilicosphaera hulburtiana*. Reworked taxa occur in the samples with  
32  
33 256 variable abundances, never exceeding about 4% (Fig. 2).

34 257  
35

### 36 258 *Planktonic foraminifera assemblages*

37  
38 259 Planktonic foraminifera are well preserved and diversified. Relative and absolute abundances of the  
39  
40 260 most abundant/significant planktonic foraminifera taxa/ groups show comparable trends throughout  
41 261 the entire succession. *Neogloboquadrina incompta* and *Turborotalita quinqueloba* are abundant in  
42  
43 262 the lower part of the record (between 12.5 ka and about 8 ka) and undergone a strong decreasing  
44  
45 263 upward (Fig. 3). Although with lower relative and absolute abundances, *G. ruber* and *G. bulloides*  
46 264 are also abundant in this interval (Fig. 3). At about 8 ka, a prominent replacement of *G. inflata* at the  
47  
48 265 expense of *N. incompta* and *T. quinqueloba* occurs. Starting from 8 ka upwards, *G. inflata* together  
49  
50 266 with *G. bulloides* and *G. ruber*, became the most abundant taxon in the record (Fig. 3). *Globigerinita*  
51  
52 267 *glutinata*, with relative abundances not higher than 10%, doesn't show any relevant fluctuation in the  
53 268 distribution pattern (Fig. 3). *Trilobatus sacculifer* became more abundant from about 8 ka upward,  
54  
55 269 showing a more prominent increase, as relative and absolute abundances, during the last 3.5 kyr (Fig.  
56  
57 270 3). A similar distribution pattern is also shown by *Truncorotalita truncatulinoidea* (Fig. 3). Other taxa  
58  
59 271 showing a very scattered distribution in the studied interval, with relative abundances < 3 % and any  
60

1

2

3 272 significant fluctuations, are not shown in Fig. 3. They are represented by *Globorotalia scitula*,  
4  
5 273 *Globigerina falconensis*, *G. rubescens*, *N. pachyderma*, *G. siphonifera* and *O. universa*.

6

7 274

### 8 275 *Sea Surface Temperature*

9

10 276 Annual, summer and winter SST patterns show sharp fluctuations between 10.2 ka and 8.7 ka  
11  
12 277 characterized by strong drops of winter and summer temperature values greater than 10°C (Fig. 3).  
13  
14 278 During this interval an important increase of *T. quinqueloba* is observed, together with high  
15  
16 279 occurrence of *N. incompta* and *N. dutertrei* and increasing trend of warm water foraminifera taxa  
17  
18 280 (Fig. 5). In this interval, the similarity index slightly decreases (Fig. 3), indicating that this species  
19  
20 281 combination is not usual in the modern oceanographic condition for the North Atlantic and the  
21  
22 282 Mediterranean region. In this interval the average annual SST is about 13.9°C, while average winter  
23  
24 283 and summer temperatures are 11.7°C and 16.7°C respectively (Fig. 3). For the last 8 kyr, the average  
25  
26 284 annual SST is about 18.5°C, while winter SST in the Alboran Sea varies around ca. 15 °C, in  
27  
28 285 agreement with modern conditions (15.4 °C; Locarnini et al., 2013) (Fig. 3). The average summer  
29  
30 286 SST is 22.6°C, exceeding modern ones (21.4°C; Locarnini et al., 2013) (Fig. 3). Low temperatures  
31  
32 287 values are recorded between about 8.6 and 7.7 ka both in summer (ca. 20°C) and in winter (ca.13°C)  
33  
34 288 (Fig. 3). The highest temperatures are recorded between 7.7 ka and 5.8 ka with temperatures up to 23  
35  
36 289 °C during summer and up to 16 °C during winter (Fig. 3). During the last 5 kyr, summer SST weakly  
37  
38 290 decreases, with slightly oscillating values between 22°C and 23°C (Fig. 3). In the same interval,  
39  
40 291 winter SSTs are almost stable with average values of about 15°C (Fig. 3), although during the last 3  
41  
42 292 kyr, the winter temperatures are characterized by a slight increase.

43 293 These results suggest that, with the exception of the interval between 10.2 and 8.7 ka, our SST record  
44  
45 294 shows values comparable with those derived from the alkenone-SST at the same site (Martrat et al.,  
46  
47 295 2014), with the foram-based SST from other nearby records (Pérez-Folgado et al., 2003; Schirrmacher  
48  
49 296 et al., 2019), and with the present-day SST in the region (Locarnini et al., 2013). On the basis of these  
50  
51 297 considerations, only the last 8.6 kyr record has been considered for the climate interpretation.

48 298

49

### 50 299 *Power spectral and wavelet analysis*

51 300 The power spectrum of total NAR shows prominent peaks (over the 95% Confidence Level – C.L.)  
52  
53 301 of periodicity ranging between 1100 yr and 1700 yr (IMF3) (Fig. 4a, c). The wavelet analysis reveals  
54  
55 302 that periodicities are not evenly distributed through time and specifically the 1102 yr cycle occurs  
56  
57 303 from 12 ka to about 4 ka (Fig. 4c), while the 1693 yr periodicity emerges since about 5 ka upwards  
58  
59 304 (Fig. 4c). Significant peaks (over the 95% of C.L.) are observed at the periods of ~ 4300 yr and ~

60

1  
2  
3 305 8000 yr all along the record (IMF 4, 5) (Fig. 4 d,e). Scattered distribution of cycles between ~ 400  
4  
5 306 and ~ 700 yr are also observed (IMF 2) (Fig. 4b).

6  
7 307

## 8 308 **Discussion**

### 10 309 *Main hydrographic and climate variations*

11  
12 310 Surface water modifications occurring in the last 11 ka can be described by three main long-term  
13  
14 311 (between 3-5000 c.a. years-long) steps: Phase I, II and III (Figs. 5-6).

15 312

### 17 313 *Phase I – the early Holocene humid period*

18  
19 314 This phase straddles the early Holocene, between 11.5 ka and 8 ka and is subsequent to the Younger  
20  
21 315 Dryas Stadial. The climate evolution of the latter stadial has been discussed in detail in Bazzicalupo  
22 316 et al. (2018) based on the same proxies and therefore not discussed in the present study. Phase I is  
23  
24 317 marked by a gradual surface water temperature increase, well described by progressively growing  
25  
26 318 abundances of both coccolithophore and foraminifera warm-water taxa, associated with increasing  
27 319 summer insolation (Fig. 5). During this phase, the distinct increase in both *Syracosphaera* spp. and  
28  
29 320 *T. quinqueloba* (Fig. 5) provides evidences of enhanced riverine/detrital input in surface waters.  
30  
31 321 *Syracosphaera* spp. has been, in fact, related to enhanced supply of fresher and turbid upper layer  
32  
33 322 (Ausín, et al., 2015b; Bazzicalupo et al., 2018; Colmenero-Hidalgo et al., 2004; Weaver and Pujol,  
34 323 1988), while the cold taxon *T. quinqueloba* flourishes in high fertile and low density surface waters  
35  
36 324 (Aksu et al., 2002; Hemleben et al., 1985; Pujol and Vergnaud-Grazzini, 1995; Triantaphyllou et al.,  
37  
38 325 2010). Enhanced abundances of this taxon have been also related to areas influenced by continental  
39  
40 326 runoff (Bartels-Jónsdóttir et al., 2015; Girone et al., 2013; Jonkers et al., 2010; Margaritelli et al.,  
41 327 2016; Rohling et al., 1997; Vallefucio et al., 2012) and, in the Eastern Mediterranean, the increase in  
42  
43 328 abundance of *T. quinqueloba*, during the deposition of sapropel layer S1, has been linked to a high  
44  
45 329 tolerance for low salinity and highly stratified water conditions coupled with the presence of high  
46 330 nutrients and terrestrial organic material (Capotondi et al., 2004; Kontakiotis, 2016; Principato et al.,  
47  
48 331 2006; Rohling et al., 1997; Zachariasse et al., 1997). The high abundance of small *Gephyrocapsa*  
49  
50 332 during phase I (Fig. 6), also sustains nutrient availability in surface water (Gartner et al., 1987;  
51  
52 333 Hernández-Almeida et al., 2011; Okada and Wells, 1997; Takahashi and Okada, 2000). A  
53 334 concomitant expansion of *Quercus* during phase I (Fig. 5) highlights enhanced humidity on land  
54  
55 335 (Combourieu-Nebout et al., 2009) likely in relation with extreme seasonality during precession  
56  
57 336 minima/insolation maxima (Fig. 5) and increased autumn/winter westerlies-carried rains over the  
58  
59 337 western Mediterranean, which supports enhanced supply of fresher water into the basin. This scenario  
60 338 seems to reflect a regional climate condition since it is consistent with the establishment of the Early

1  
2  
3 339 Holocene humid phase, occurring between 11.5 and 7 ka (Jalut et al., 2009; Magny et al., 2002, 2013;  
4  
5 340 Peyron et al., 2017; Zanchetta et al., 2007; Zielhofer et al., 2017) and with additional evidences of  
6  
7 341 autumn/winter precipitation increase over the northern Mediterranean borderlands during northern  
8  
9 342 Hemisphere insolation maxima (Kutzbach et al., 2013; Meijer and Tuenter, 2007; Toucanne et al.,  
10 343 2015; Tzedakis, 2007). Phase I is within the interval of sapropel layer S1 deposition in the Eastern  
11  
12 344 Mediterranean (10.8-6.1 ka, De Lange et al., 2008), developed during maximum summer insolation,  
13  
14 345 that contributed, through the enhanced monsoon precipitation, to increased runoff in the Eastern  
15 346 Mediterranean (Howell and Thunell, 1992; Rohling et al., 2002, 2004, 2015; Rossignol-Strick, 1985;  
16  
17 347 Rossignol-Strick et al., 1982). Our data evidence that freshwater runoff during sapropel events was  
18  
19 348 not restricted to the Eastern Mediterranean but was rather widespread over the entire Mediterranean  
20  
21 349 Sea due to increased rainfall (Bard et al., 2002; Kallel et al., 2000; Kallel and Labeyrie, 1997;  
22 350 Toucanne et al., 2015; Zanchetta et al., 2007), thus strengthening the connection between North  
23  
24 351 African summer monsoon and the increased western Mediterranean autumn/winter precipitation  
25  
26 352 during sapropel deposition (Toucanne et al., 2015). On the other hand, phase I straddles the final  
27 353 phase of the deposition of ORL 1 as indicated by the decreasing, albeit still high, values of  $C_{37}$  (Fig.  
28  
29 354 5), and reduced deep water ventilation in the western Mediterranean (Frigola et al., 2007). Given the  
30  
31 355 time offset between the beginning of the ORL1 formation (14.5 ka, Martrat et al., 2014), and the  
32  
33 356 recorded enhanced riverine input and humidity on land at c.a. 11.5 ka, it appears unlikely that excess  
34 357 precipitation was the driving force of the ORL1 formation in the western Mediterranean (Rogerson  
35  
36 358 et al., 2008). As stated in Bazzicalupo et al. (2018), shoaling of the nutricline and increased export  
37  
38 359 production at the sea floor are relevant mechanism in the ORL1 deposition at the study core.

#### 39 360 40 41 361 *The 8.2 ka event*

42  
43 362 The transition between phase I and the following phase II is characterized by higher absolute  
44  
45 363 abundances of *N. incompta* between ~8.6 ka and ~8.1 ka (Fig. 6) and by a sharp warm water taxa  
46  
47 364 decrease (Fig. 5), suggesting water cooling. In more detail, a sharp and brief cooling event of about  
48 365 3°C is recorded in annual, winter and summer SST (Fig. 6). An interruption of the surface water  
49  
50 366 warming trend is also indicated by a decrease of warm water coccolith taxa in the early stage (Fig.  
51  
52 367 5). A concomitant temperate forest regression (Fig. 6) marks a short-term precipitation decrease  
53 368 episode.

54  
55 369 This cooling episode is here related to the well-known cold and dry 8.2 ka event that punctuates the  
56  
57 370 early Holocene evolution and it is broadly recognized in Greenland ice core records (Alley and  
58  
59 371 Ágústsdóttir, 2005; Bond et al., 1997, 2001; Dansgaard et al., 1993; Lowe et al., 2008; Rasmussen et  
60 372 al., 2006; Rohling and Pälike, 2005) and in the Mediterranean (e.g. De Rijk et al., 1999; Lirer et al.,

1  
2  
3 373 2013; Rohling et al., 2002; Sprovieri et al., 2003). In the ODP Site 976, the modification of the water  
4  
5 374 column structure indicated by calcareous plankton can be related to a southward displacement of the  
6  
7 375 ITCZ (Intertropical Convergence Zone) and an intensified impact of harsher, higher-latitude climate  
8  
9 376 conditions in the Mediterranean region (Rohling et al., 2002, 2004). Today, *N. incompta* does not  
10 377 dwell in the Alboran Sea due to the occurrence of deep pycnocline and nutricline (located at a depth  
11  
12 378 of about 150-200m) and winter temperatures reaching 15°C (Pujol and Vergnaud Grazzini, 1995;  
13  
14 379 Rohling et al., 1995). On the other hand, this taxon is abundant in the Gulf of Lion where strong  
15 380 winter mixing facilitates the advection of nutrients into the euphotic zone and, mainly, winter  
16  
17 381 temperatures reach 12°C (Pujol and Vergnaud-Grazzini, 1995; Rohling et al., 1995).  
18  
19 382 The marked increase of coccolithophore production within the upper part of the 8.2 ka event, as  
20  
21 383 indicated by the peak in total NAR (Fig. 2), is likely the result of an important hydrographic  
22 384 modification occurring at this time, related to the enhanced Atlantic water inflow. This feature marks  
23  
24 385 the onset of the following phase II as discussed below and is very well comparable with a similar  
25  
26 386 peak in the coccolithophore absolute abundance at 8.2 ka recorded in the Alboran Sea by Colmenero-  
27 387 Hidalgo et al. (2004) and related to the onset of gyre circulation into the basin.  
28  
29 388  
30  
31 389 *Phase II: the middle Holocene establishment of the modern oceanographic circulation*  
32  
33 390 Phase II represents the second major step in the hydrographic evolution of the basin. It develops  
34 391 between 8.2 ka and about 5.3 ka, thus it nearly represents the middle Holocene portion of the record  
35  
36 392 (Bárcena et al., 2004; Giraudeau, 1993). It is marked by a distinct abundance increase of *F. profunda*  
37  
38 393 and a subsequent increase of *G. inflata* (Fig. 6) which replaces *N. incompta*. *Florisphaera profunda*  
39 394 is a deep photic zone dweller and thrives with a deep nutricline and water column stratification  
40  
41 395 (Baumann et al., 2005; Incarbona et al., 2013; Sprovieri et al., 2012), while *G. inflata* is a deep living  
42  
43 396 taxon and benefits from water column stability, a deep pycnocline and reduced upwelling conditions.  
44  
45 397 The shift between *G. inflata* and *N. incompta* is in agreement with Rohling et al. (1995) that linked  
46 398 this event to the establishment of the modern front-dominated conditions in the Alboran Sea, when  
47  
48 399 the amount of Atlantic water inflow was close to the present volume. At Site 976, the enhanced  
49  
50 400 Atlantic inflow, following the deglaciation and the sea level rise, would have deepened the nutricline  
51  
52 401 favoring *F. profunda*. In addition, it would have promoted both the development of the modern  
53 402 geostrophic front, where *G. inflata* proliferates (Pujol and Vergnaud-Grazzini, 1995; Rohling et al.,  
54  
55 403 1995) and the establishment of WAG (Ausín et al., 2015b; Pérez-Folgado et al., 2003; Rohling et al.,  
56  
57 404 1995). This hydrographic evolution follows the culmination of the highest rate of global sea-level  
58 405 rise (Lambeck et al., 2014). Concurrently to the development of a deep nutricline, high annual and  
59  
60 406 seasonal SSTs are recorded (Fig. 6) also marked by the increase of the tropical taxon *T. sacculifer*

1  
2  
3 407 (Fig. 6). Conversely, small *Gephyrocapsa* and neogloboquadrinids decrease (Fig. 6). We suggest that  
4  
5 408 anomalous sea-surface warmer conditions during this period promoted a prolonged water column  
6  
7 409 stratification, deepening of the thermocline (nutricline) and decrease of winter wind-induced mixing.  
8  
9 410 These conditions contributed to a higher increase of warm and oligotrophic taxa, that currently thrives  
10 411 during mid-summer in the Mediterranean Sea (Bárcena et al., 2004; Pujol and Vergnaud-Grazzini,  
11  
12 412 1995), and decreasing of those taxa more related to nutrient-rich conditions such as small  
13  
14 413 *Gephyrocapsa* and neogloboquadrinids. The occurrence of *G. bulloides* during this phase (Fig. 6) is  
15 414 consistent with its opportunistic behavior (Pujol and Vergnaud-Grazzini, 1995; Rohling et al., 1997;  
16  
17 415 Schiebel et al., 2001) and its favorite habitat, highly dependent on enhanced food availability, related  
18  
19 416 to strong seasonal contrast or river input. High abundances of temperate forest in the early stage of  
20  
21 417 phase II (Fig. 6) suggest still wet climate conditions on land. This phase, although coeval with the  
22 418 younger portion of S1, is subsequent to the end of ORL 1 deposition in the Alboran Sea (Fig. 5). Deep  
23  
24 419 anoxia in the western basin is in fact independent of that of the eastern basin (Rogerson et al., 2008)  
25  
26 420 and ORL 1 termination is related to the 8.2 ka event and to the establishment of the modern front-  
27  
28 421 dominated conditions in the western Mediterranean (Cacho et al., 2002; Rogerson et al., 2008).  
29 422 During phase II, differently from phase I occurring during ORL1 deposition and characterized by  
30  
31 423 shoaling of the nutricline and enhanced productivity in surface water (Bazzicalupo et al., 2018), the  
32  
33 424 calcareous plankton assemblages indicate stratified conditions in column water and deep nutricline,  
34 425 which likely prevented productivity in surface water and export production at the sea floor. This  
35  
36 426 datum supports the hypothesis that productivity, although does not represent the triggering  
37  
38 427 mechanism, may provide a secondary control in the ORL formation (Rogerson et al., 2008).  
39  
40 428

### 41 429 *Phase III: the late Holocene reduced seasonality*

42  
43 430 This phase is marked by the coeval increase of small *Gephyrocapsa* and *G. bulloides*, at c.a. 5.3 ka  
44  
45 431 (Fig. 6), suggesting increased nutrient availability in surface waters. These taxa are, in fact,  
46  
47 432 considered high surface water productivity proxies (Barcena et al., 2004; Colmenero-Hidalgo et al.,  
48 433 2004; Gartner et al., 1987; Pujol and Vergnaud-Grazzini, 1995 Takahashi and Okada, 2000). The  
49  
50 434 enhanced abundances of the deep mixed dweller *T. truncatulinoides* (Fig. 6) support more intense  
51  
52 435 seasonal and prolonged mixing. Elevated abundances of *T. truncatulinodes* from sediment trap in the  
53 436 Gulf of Lions have been related to increased winter mixing conditions (Rigual-Hernández et al.,  
54  
55 437 2012). On the other hand, the high abundance of *F. profunda* and *G. inflata* (Fig. 6) is still in relation  
56  
57 438 with the modern front-dominated conditions in the Alboran Sea and deep nutricline, originating at  
58  
59 439 the onset of phase II. Oscillations in the absolute abundances of *F. profunda* as well as of small  
60 440 *Gephyrocapsa* (Fig. 6) are likely in relation with short-term fluctuations in total NAR, which are

1  
2  
3 441 discussed in more detail below. Foraminifera warm-water taxa, together with *G. ruber* group and to  
4  
5 442 a less degree warm water coccolith taxa, show a general decreasing trend (Fig. 5). The summer SST  
6  
7 443 record (Fig. 6) is in line with reducing summer insolation trend (Fig. 5) and with evidence from the  
8  
9 444 western Mediterranean terrestrial record of reduced seasonality (cooler summers and warmer winters)  
10 445 during the transition to late Holocene (Ramos-Román et al., 2018). The aridification process,  
11  
12 446 accompanying the reduced seasonality at this time is highlighted, in the pollen record, by an increase  
13  
14 447 in *Artemisia* at around 4 ka at the studied core (Fig. 6), and by several coeval Mediterranean records  
15 448 (Desprat et al., 2013; Fletcher et al., 2012; Fletcher and Sánchez Goñi, 2008; Jalali et al., 2016; Jalut  
16  
17 449 et al., 2000, 2009; Magny et al., 2013; Ramos-Román et al., 2018).

18  
19 450 The last 3.5 kyr of phase III are marked by a relevant increase of *T. sacculifer* (Fig. 6). The distribution  
20  
21 451 pattern of this taxon is punctuated by three main short-term pulses (Ts1-Ts3 in Fig. 6), not previously  
22 452 recorded in the western Mediterranean. *Trilobatus sacculifer* mainly occurs in warm and oligotrophic  
23  
24 453 tropical and sub-tropical waters with low seasonality (Bé and Hutson, 1977; Fraile et al., 2008;  
25  
26 454 Hemleben et al., 1989; Vincent and Berger, 1981). Today this taxon reaches its maximum abundance  
27 455 in the Eastern Mediterranean basin and in the Red Sea, where low nutrient and warm surface waters  
28  
29 456 prevail throughout the year, due to the relatively stable deep pycnocline (Kallel and Labeyrie, 1997;  
30  
31 457 Kucera et al., 2005; Pujol and Vergnaud-Grazzini, 1995; Siccha et al., 2009). In the Red Sea, its  
32  
33 458 increasing trend, during the Holocene, has been also related to more arid conditions during reduced  
34 459 monsoon climate system and prevailing eastern Mediterranean climate system (Edelman-Furstenberg  
35  
36 460 et al., 2009). In our record, the last 3.5 kyr are characterized by a reduction of seasonal thermal  
37  
38 461 gradient ( $\Delta\text{SST}_{\text{sum-win}}$ , Fig. 6) in the seawater, likely related to weak increase of winter SST,  
39  
40 462 concomitant with ameliorate climate condition on land, as suggested by coeval relative increases of  
41 463 temperate forests in the pollen assemblages (Fig. 6). A positive correlation between *T. sacculifer* and  
42  
43 464 weaker winter conditions and stratification has been also found in the Arabian Sea (Munz et al.,  
44  
45 465 2015). We suggest that, at Site 976, relatively higher winter SSTs (with values exceeding 15°C) with  
46  
47 466 respect to the earlier interval, developed more stable year-round surface water conditions in the basin  
48 467 favoring the increase of *T. sacculifer* in the last 3.5 kyr. Such conditions could probably represent the  
49  
50 468 response to changes in hydrological conditions in the adjacent Iberian basin, related to the reduction  
51  
52 469 of meltwater discharge in the North Atlantic (Bond et al., 2001). In the Gulf of Cádiz, according to  
53 470 Schirrmacher et al. (2019), larger seasonal SST contrasts, during the Holocene, are related to periods  
54  
55 471 of enhanced iceberg discharge; the northward heat transport was blocked due to freshwater forcing  
56  
57 472 in the North Atlantic resulting in colder winter temperatures and higher summer temperatures due to  
58  
59 473 a seasonal northward migration of Intertropical Convergence Zone (ITCZ). This mechanism is similar  
60 474 to the one proposed by Repschläger et al. (2017) for the early Holocene, when reinforcements of



1  
2  
3 475 northward heat transport and migration of Subtropical Gyre is found during periods of weak north  
4  
5 476 Atlantic meltwater discharge. Similarly, we retain that the decrease in the drift ice index during the  
6  
7 477 last 3 kyr (Bond et al., 2001), could have promoted higher northward advection of warmer water  
8  
9 478 masses that could have also reached the Alboran Sea through the Strait of Gibraltar, favoring the  
10 479 instauration of a lower seasonal thermal gradient. The three distinct peaks of *T. sacculifer*, centered  
11  
12 480 at about 2.9 ka, 1.8 ka and 0.7 ka, trace the occurrence of short warm pulses at the core location. They  
13  
14 481 appear chronologically correlated with the short-term warm and dry events identified in northwestern  
15 482 Africa lakes and in the Adriatic Sea (Piva et al., 2008; Zielhofer et al., 2017). The phase Ts1 is also  
16  
17 483 chronologically correlated with the warm phase recognized by Margaritelli et al. (2016) during the  
18  
19 484 Middle Bronze Age–Iron Age in the central Mediterranean.

### 20 485 21 22 486 *Millennial scale variations*

23  
24 487 Since the WAG establishment in the Alboran Sea at ca. 8 ka, total NAR values show a series of  
25  
26 488 millennial-scale fluctuations over the middle and late Holocene at Site 976 (Fig. 7). This pattern  
27  
28 489 indicates that high-frequency variations in the coccolithophore productivity are superimposed to the  
29 490 main climate phases. Connecting coccolithophore productivity to environmental proxies is a complex  
30  
31 491 task since multiple relationships might affect the link between the various signals. A certain  
32  
33 492 chronological uncertainty is also added, when comparing different sites with different age models. In  
34 493 order to unravel the forcing mechanism responsible for coccolithophore productivity variations at the  
35  
36 494 studied core, we compared a few coccolithophore proxies with the pattern of  $\delta^{18}\text{O}_{\text{seawater}}$  available at  
37  
38 495 the ODP Site 976 (Jiménez-Amat and Zahn, 2015), as a proxy of local surface water salinity variation.  
39  
40 496 We have also performed a comparison with the detrended  $\delta^{18}\text{O}_{\text{speleothem}}$  curve (Smith et al., 2016),  
41 497 which represents a high-resolution archive of quasi-cyclical events of relatively wet-to-dry climatic  
42  
43 498 conditions over Iberia, with a ~1500 year frequency (Smith et al., 2016). This trend is significantly  
44  
45 499 correlated with the NAO index (Olsen et al., 2012) (Fig. 7). A relationship between coccolithophore  
46  
47 500 productivity and NAO modes has been recently suggested in the Alboran Sea by Ausín et al. (2015a).  
48 501 These authors indicate weakened (intensified) upwelling, related to weaker (stronger) westerlies,  
49  
50 502 responsible for reduced (reinforced) WMDW in the Gulf of Lions. In this scenario, the NAO  
51  
52 503 circulation mode is the forcing mechanism of coccolithophore variability. Intensified upwelling  
53 504 would have been promoted by stronger westerlies blowing over the Gulf of Lions, during a NAO –  
54  
55 505 mode. These conditions would have promoted major WMDW formation and simultaneous  
56  
57 506 enhancement of the AJ influx, both fluctuating in-phase (Ausín et al., 2015a; García Lafuente et al.,  
58  
59 507 2002, 2007) . The AJ would have migrated southward, allowing the cool subsurface waters to fill the  
60 508 area left behind the jet (Sarhan, 2000) and thus promoting upwelling. In the present work, a first

1  
2  
3 509 comparison between datasets indicates that low salinity phases (lighter  $\delta^{18}\text{O}_{\text{seawater}}$ ) are concurrent  
4  
5 510 with high values of *G. oceanica* (Fig. 7). The occurrence of *G. oceanica* within the western  
6  
7 511 Mediterranean basin has been often related to Atlantic surface water inflows (Álvarez et al., 2010;  
8  
9 512 Bárcena et al., 2004; Bazzicalupo et al., 2018; Knappertsbusch, 1993; Oviedo et al., 2017). The  
10 513 positive correlation of the coccolithophore taxon with salinity minima at Site 976, further supports  
11  
12 514 the relation between *G. oceanica* and Atlantic surface water inflows, since salinity minimum in the  
13  
14 515 Alboran Sea essentially traces phases of enhanced Atlantic water into the basin (Font et al., 1998;  
15 516 Sarhan et al., 2000; Viúdez et al., 1996). Consequently, we use the lighter values of  $\delta^{18}\text{O}_{\text{seawater}}$  and  
16 517 the increased abundance of *G. oceanica* as proxies of Atlantic inflow in the Alboran Sea (Fig. 7),  
17 518 which both provide a regime of cyclical Atlantic water inflow intensity in the basin. Coccolithophore  
18  
19 519 productivity variations, expressed as total NAR, display distinct pulses, well-correlated with the  
20  
21 520 pattern of the changing Atlantic inflow intensity and with the concomitant occurrence of alternating  
22 521 dry/wet phases in the Iberia  $\delta^{18}\text{O}_{\text{speleothem}}$  (Fig. 7). Therefore, the various proxies point out to a  
23  
24 522 coupling between enhanced coccolithophore productivity (high total NAR values), intensified  
25 523 Atlantic waters inflow (lighter  $\delta^{18}\text{O}_{\text{seawater}}$  and increased abundance of *G. oceanica*), and arid  
26 524 conditions over the Iberia Peninsula (peaks in  $\delta^{18}\text{O}_{\text{speleothem}}$ ), correlated with NAO+ phases (Fig. 7).  
27  
28 525 Our data support the model proposed by Ausín et al. (2015a), and specifically the relation between  
29 526 coccolithophore productivity, Atlantic inflow and WMDW strength, although the dataset at site 976  
30  
31 527 indicate an opposite relationship between coccolithophore productivity and NAO mode. According  
32  
33 528 to the present results, enhanced Atlantic water inflow occurred during a persistent NAO+ index (Fig.  
34 529 7); the latter would have strengthened the north-westerlies over the northwestern Mediterranean  
35 530 basin, promoting a reinforcement of deepwater overturning and in turn increased the AJ (Fig. 8). The  
36 531 suggested relation between NAO mode and WMDW strength is in agreement with results from  
37 532 today's survey in the western Mediterranean (Rixen et al., 2005) and with the proposed relationship  
38 533 between strengthening of the WMDW and NAO variability in the past. In fact, during the Holocene  
39 534 and the Dansgaard-Oeschger events NAO + phases would have strengthen the northwesterlies over  
40 535 the northwestern Mediterranean, enhancing the WMDW formation (Frigola et al., 2007; Moreno et  
41 536 al., 2002, 2004, 2005; Nieto-Moreno et al., 2011). The scenario is also consistent with the observed  
42 537 decadal-variability between NAO intensity and upwelling strength highlighted in the western  
43 538 Mediterranean (Vargas-Yáñez et al., 2008). A possible reasonable explanation for the differing  
44 539 interpretations between the present work and the Ausín et al. (2015a) study, is that the latter authors  
45 540 based their paleoceanographic reconstruction on oscillations of the *F. profunda* NAR abundances in  
46 541 the Alboran Sea. In Ausín et al. (2015a), *F. profunda* NAR peaks have been linked to the  
47 542 intensification of the upwelling conditions in the area. Recent data establish a precise relationship

1  
2  
3 543 between *F. profunda* and primary productivity levels in today's low-latitude oceans (Hernández-  
4  
5 544 Almeida et al., 2019) and suggest that the link between *F. profunda* abundance and net primary  
6  
7 545 productivity in the Mediterranean Sea is not straight forward thus discouraging the use of this taxon  
8  
9 546 as a productivity indicator into the basin (Hernández-Almeida et al., 2019).

#### 10 547 11 12 548 *External and internal forcing mechanisms of coccolithophore productivity cycles*

13 549 The time series analysis performed on the total NAR record confirms the occurrence of millennial-  
14  
15 550 scale periodicities in coccolithophore productivity during the Holocene and highlights two main  
16  
17 551 periodicities through the record: the first one of ~ 1100 yr (from 12.5 to c.a. 5 ka) and the second one  
18  
19 552 of ~ 1700 yr (from 5 to 0.19 ka) (Fig. 4c). The results of spectral and wavelength analyses indicate  
20  
21 553 that coccolithophore productivity changes in the Alboran Sea were modulated both by external (solar)  
22 554 and internal (oceanic-atmospheric) forcing. In fact, the ~ 1100 yr-cycles appear close to the ~ 1000  
23  
24 555 yr cycle identified during the early Holocene in solar proxies in North Atlantic records and in IRD  
25  
26 556 record (Debret et al., 2007, 2009). They are also detected in the western Mediterranean pollen record,  
27  
28 557 which displays a periodic component of ~ 900 yr (Fletcher et al., 2012) and of ~ 1100 yr (Ramos-  
29 558 Román et al., 2018) during the early and middle Holocene. On the other hand, cycles of ~ 1700 yr  
30  
31 559 are very close to the 1600-year cycle dominating the last 5000 yr in several paleoclimate  
32  
33 560 records (Debret et al., 2007; 2009 and references therein) and related to internal  
34 561 (oceanic/atmospheric) forcing. A similar shift in periodicity to a dominant ~ 1750 oscillation in the  
35  
36 562 last 6 ka (Fletcher et al., 2012) and ~ 1600 yr-cycle (Ramos-Román et al., 2018) in the last 4.7 ka has  
37  
38 563 been detected in the western Mediterranean in the pollen record and is related to the influence of  
39  
40 564 NAO-like circulation in the mid-late Holocene. The similar pattern in cyclicity observed in the  
41 565 present study in NAR pattern in the Alboran Sea strengthens the relation between coccolithophore  
42  
43 566 productivity/hydrographic changes and atmospheric variability modulated by NAO fluctuations and  
44  
45 567 sustains the occurrence of a periodicity change through the Holocene from a dominant external (solar)  
46 568 to a dominant internal (oceanic/atmospheric) forcing.  
47

#### 48 569 49 50 570 **Conclusions**

51 571 The calcareous plankton assemblage (coccolithophore and foraminifera) of the ODP Site 976 from  
52  
53 572 the Alboran Sea has been studied at a centennial-scale resolution, to investigate the climate variability  
54  
55 573 and the forcing mechanisms affecting the western Mediterranean basin during the last 12.5 ka.  
56  
57 574 Coccolithophore and planktonic foraminifera dataset is integrated with pollen and geochemical data  
58 575 available at the site. During a first step, between 11.5 and 8.2 ka, calcareous plankton assemblage  
59  
60 576 clearly traces increasing temperature and freshwater arrival, related to riverine input in the basin,

1  
2  
3 577 during a period of insolation maxima. The timing of this phase in the Alboran Sea is quasi  
4  
5 578 concomitant with sapropel S1 deposition in the eastern Mediterranean, suggesting a connection  
6  
7 579 between the monsoonal mechanism for sapropel formation and high rainfall conditions in  
8  
9 580 Northwestern Europe. Following an abrupt surface water temperature decrease correlated with  
10 581 humidity reduction and centered at 8.2 ka, the second phase (8-4.6 ka) is marked by a profound  
11  
12 582 change in the planktonic assemblages, reflecting a more stratified water column, the deepening of the  
13  
14 583 nutricline following a sea level rise and the instauration of the modern gyre circulation. The third  
15 584 final phase (4.6-0.19 ka) is characterized by reduced seasonality (cooler summers and warmer  
16  
17 585 winters), enhanced surface water mixing and increased aridification on land related with a decrease  
18  
19 586 in summer insolation. Short-term cyclicality occurs in coccolithophore productivity, with a clear pattern  
20  
21 587 mainly occurring since the establishment of the modern circulation. Millennial-cycles of increased  
22 588 coccolithophore productivity are associated with enhanced inflows of Atlantic water from the  
23  
24 589 Gibraltar strait modulated by NAO+ mode. The proposed scenario strengthens the role of  
25  
26 590 hydrographic changes and atmospheric variability modulated by NAO fluctuations on  
27 591 coccolithophore productivity in the Alboran Sea. The results of the spectral analysis add information  
28  
29 592 on the value of coccolithophores in recording environmental changes and highlight that  
30  
31 593 coccolithophore productivity is modulated by both external (solar) and internal (oceanic-  
32  
33 594 atmospheric) forcing. A shift in periodicity from a dominant ~ 1100 yr oscillations to ~ 1600 yr  
34 595 periodicity occurs at about 4 ka and appears in agreement with enhanced influence of NAO-like  
35  
36 596 circulation during the late Holocene.

37  
38 597

### 39 598 **Acknowledgements**

41 599 Two anonymous reviewers are greatly acknowledged for their valuable contributions which improved  
42  
43 600 the early version of this manuscript. The authors thank the Ocean Drilling Program for providing the  
44  
45 601 samples of ODP Site 976. This research was financially supported by the Geoscience PhD  
46 602 scholarship, Università degli Studi di Bari, and benefited of instrumental upgrades from  
47  
48 603 “Potenziamento Strutturale PONA3\_00369 dell'Università degli Studi di Bari, Laboratorio per lo  
49  
50 604 Sviluppo Integrato delle Scienze e delle Tecnologie dei Materiali Avanzati e per dispositivi innovativi  
51 605 (SISTEMA). E.S. was funded by a postdoctoral fellowship (SFRH/ BPD/111433/2015) from  
52  
53 606 Fundação para a Ciência e a Tecnologia (FCT).

54  
55 607

### 56 608 **References**

58 609

60 610 Aksu AE, Hiscott RN, Kaminski MA, et al. (2002) Last glacial–Holocene paleoceanography of the

1

2

3 611

Black Sea and Marmara Sea: stable isotopic, foraminiferal and coccolith evidence. *Marine*

4

5 612

*Geology* 190(1–2). Elsevier: 119–149. DOI: 10.1016/S0025-3227(02)00345-6.

6

7

8 613

Alley RB and Ágústsdóttir AM (2005) The 8k event: Cause and consequences of a major Holocene

9 614

abrupt climate change. *Quaternary Science Reviews* 24(10–11): 1123–1149. DOI:

10

11 615

10.1016/j.quascirev.2004.12.004.

12

13

14 616

Álvarez MC, Amore OF, Cros LL, et al. (2010) Coccolithophore biogeography in the

15 617

Mediterranean Iberian margin. *Revista Española de Micropaleontología* 42(3): 359–371.

16

17

18 618

André A, Weiner A, Quillévéré F, et al. (2012) The cryptic and the apparent reversed: lack of

19

20 619

genetic differentiation within the morphologically diverse plexus of the planktonic foraminifer

21

22 620

*Globigerinoides sacculifer*. *Paleobiology* 39(01). GeoScienceWorld: 21–39. DOI:

23

24 621

10.1666/0094-8373-39.1.21.

25

26 622

Aurahs R, Treis Y, Darling K, et al. (2011) A revised taxonomic and phylogenetic concept for the

27

28 623

planktonic foraminifer species *Globigerinoides ruber* based on molecular and morphometric

29

30 624

evidence. *Marine Micropaleontology* 79(1–2). Elsevier: 1–14.

31

32 625

Ausín B, Flores JA, Sierro FJ, Cacho I, et al. (2015a) Atmospheric patterns driving Holocene

33

34 626

productivity in the Alboran Sea (Western Mediterranean): A multiproxy approach. *The*

35

36 627

*Holocene* 25(4): 583–595. DOI: 10.1177/0959683614565952.

37

38

39 628

Ausín B, Flores JA, Sierro FJ, Bárcena MA, et al. (2015b) Coccolithophore productivity and

40

41 629

surface water dynamics in the Alboran Sea during the last 25kyr. *Palaeogeography,*

42

43 630

*Palaeoclimatology, Palaeoecology* 418. Elsevier B.V.: 126–140. DOI:

44

45 631

10.1016/j.palaeo.2014.11.011.

46

47 632

Bárcena MA, Cacho I, Abrantes F, et al. (2001) Paleoproductivity variations related to climatic

48

49 633

conditions in the Alboran Sea (western Mediterranean) during the last glacial-interglacial

50

51 634

transition: The diatom record. *Palaeogeography, Palaeoclimatology, Palaeoecology* 167(3–4):

52

53 635

337–357. DOI: 10.1016/S0031-0182(00)00246-7.

54

55 636

Bárcena MA, Flores JA, Sierro FJ, et al. (2004) Planktonic response to main oceanographic changes

56

57 637

in the Alboran Sea (Western Mediterranean) as documented in sediment traps and surface

58

59 638

sediments. *Marine Micropaleontology* 53(3–4): 423–445. DOI:

60

60 639

10.1016/j.marmicro.2004.09.009.

- 1  
2  
3 640 Bard E, Delaygue G, Rostek F, et al. (2002) Hydrological conditions over the western  
4  
5 641 Mediterranean basin during the deposition of the cold Sapropel 6 (ca. 175 kyr BP). *Earth and*  
6  
7 642 *Planetary Science Letters* 202(2). Elsevier: 481–494. DOI: 10.1016/S0012-821X(02)00788-4.  
8  
9 643 Bartels-Jónsdóttir HB, Voelker AHL, Abrantes FG, et al. (2015) High-frequency surface water  
10  
11 644 changes in the Tagus prodelta off Lisbon, eastern North Atlantic, during the last two millennia.  
12  
13 645 *Marine Micropaleontology* 117. Elsevier: 13–24. DOI: 10.1016/J.MARMICRO.2015.03.001.  
14  
15 646 Baumann K-H, Boeckel B, Frenz M, et al. (2004) Coccolith contribution to South Atlantic  
16  
17 647 carbonate sedimentation; Coccolithophores; from molecular processes to global impact. In:  
18  
19 648 *Coccolithophores - From Molecular Processes to Global Impact*, pp. 367–402. DOI:  
20  
21 649 10.1016/S0079-6352(99)80122-2.  
22  
23 650 Baumann K-H, Andruseit H, Böckel B, et al. (2005) The significance of extant coccolithophores as  
24  
25 651 indicators of ocean water masses, surface water temperature, and palaeoproductivity: a review.  
26  
27 652 *Paläontologische Zeitschrift* 79(1): 93–112. DOI: 10.1007/BF03021756.  
28  
29  
30 653 Bazzicalupo P, Maiorano P, Girone A, et al. (2018) High-frequency climate fluctuations over the  
31  
32 654 last deglaciation in the Alboran Sea, Western Mediterranean: Evidence from calcareous  
33  
34 655 plankton assemblages. *Palaeogeography, Palaeoclimatology, Palaeoecology* 506. Elsevier:  
35  
36 656 226–241. DOI: 10.1016/J.PALAEO.2018.06.042.  
37  
38 657 Bé AWH and Hutson WH (1977) Ecology of Planktonic Foraminifera and Biogeographic Patterns  
39  
40 658 of Life and Fossil Assemblages in the Indian Ocean. *Micropaleontology* 23(4). The  
41  
42 659 Micropaleontology Project., Inc.: 369. DOI: 10.2307/1485406.  
43  
44 660 Boeckel B and Baumann K-H (2004) Distribution of coccoliths in surface sediments of the south-  
45  
46 661 eastern South Atlantic Ocean: Ecology, preservation and carbonate contribution. *Marine*  
47  
48 662 *Micropaleontology* 51(3–4): 301–320. DOI: 10.1016/j.marmicro.2004.01.001.  
49  
50 663 Bond G, Showers W, Cheseby M, et al. (1997) A pervasive Millennial-scale cycle in the North  
51  
52 664 Atlantic Holocene Climate. *Science* 278: 1257–1266.  
53  
54 665 Bond G, Kromer B, Beer J, et al. (2001) Persistent solar influence on North Atlantic climate.  
55  
56 666 *Science* 294(5549): 2130–2136. DOI: 10.1126/science.1065668.  
57  
58  
59 667 Cacho I, Grimalt JO, Pelejero C, et al. (1999) Dansgaard-Oeschger and Heinrich event imprints in  
60  
668 Alboran Sea paleotemperatures. *Paleoceanography* 14(6). John Wiley & Sons, Ltd: 698–705.

1  
2  
3 669 DOI: 10.1029/1999PA900044.  
4

5  
6 670 Cacho I, Grimalt JO, Canals M, et al. (2001) Variability of the western Mediterranean Sea surface  
7  
8 671 temperature during the last 25,000 years and its connection with the Northern Hemisphere  
9  
9 672 climatic change. *Paleoceanography* 16(1): 40–52. DOI: 10.1029/SP010.  
10

11  
12 673 Cacho I, Grimalt JO and Canals M (2002) Response of the Western Mediterranean Sea to rapid  
13  
14 674 climatic variability during the last 50,000 years: A molecular biomarker approach. *Journal of*  
15  
16 675 *Marine Systems* 33–34: 253–272. DOI: 10.1016/S0924-7963(02)00061-1.  
17

18 676 Capotondi L, Maria Borsetti A and Morigi C (1999) Foraminiferal ecozones, a high resolution  
19  
20 677 proxy for the late Quaternary biochronology in the central Mediterranean Sea. *Marine Geology*  
21  
22 678 153(1–4). Elsevier: 253–274. DOI: 10.1016/S0025-3227(98)00079-6.  
23

24 679 Capotondi L, Soroldoni E, Principato MS, et al. (2004) Late Quaternary planktonic foraminiferal  
25  
26 680 distributions : problems related to size fraction. *Proceedings of the First Italian Meeting on*  
27  
28 681 *Environmental Micropaleontology* (9): 1–6.  
29

30  
31 682 Català A, Cacho I, Frigola J, et al. (2018) Holocene hydrography evolution in the Alboran Sea: a  
32  
33 683 multi-record and multiproxy comparison. *Climate of the Past Discussions* 15(3): 927–942.  
34

35 684 Cita MB, Vergnaud-Grazzini C, Robert C, et al. (1977) Paleoclimatic Record of a Long Deep Sea  
36  
37 685 Core from the Eastern Mediterranean. *Quaternary Research* 8(2). Cambridge University Press:  
38  
39 686 205–235. DOI: 10.1016/0033-5894(77)90046-1.  
40

41 687 Colmenero-Hidalgo E, Flores JA and Sierro FJ (2002) Biometry of *Emiliania huxleyi* and its  
42  
43 688 biostratigraphic significance in the Eastern North Atlantic Ocean and Western Mediterranean  
44  
45 689 Sea in the last 20 000 years. *Marine Micropaleontology* 46(3–4): 247–263. DOI:  
46  
47 690 10.1016/S0377-8398(02)00065-8.  
48

49 691 Colmenero-Hidalgo E, Flores JA, Sierro FJ, et al. (2004) Ocean surface water response to short-  
50  
51 692 term climate changes revealed by coccolithophores from the Gulf of Cadiz (NE Atlantic) and  
52  
53 693 Alboran Sea (W Mediterranean). *Palaeogeography, Palaeoclimatology, Palaeoecology* 205(3–  
54  
55 694 4): 317–336. DOI: 10.1016/j.palaeo.2003.12.014.  
56

57 695 Comas M, Zahn R and Klaus A (1996) *Ocean Drilling Program LEG 161 Preliminary Report*  
58  
59 696 *Mediterranean Sea II - The Western Mediterranean. ODP Preliminary Report.*  
60

697 Combourieu-Nebout N, Turon JL, Zahn R, et al. (2002) Enhanced aridity and atmospheric high-

- 1  
2  
3 698 pressure stability over the western Mediterranean during the North Atlantic cold events of the  
4  
5 699 past 50 k.y. *Geology* 30(10): 863.  
6  
7  
8 700 Combourieu-Nebout N, Peyron O, Dormoy I, et al. (2009) Rapid climatic variability in the west  
9  
10 701 Mediterranean during the last 25 000 years from high resolution pollen data. *Climate of the*  
11 702 *Past* 5: 503–521. DOI: 10.1109/IGARSS.2010.5652499.  
12  
13  
14 703 Corselli C, Principato MS, Maffioli P, et al. (2002) Changes in planktonic assemblages during  
15  
16 704 sapropel S5 deposition: Evidence from Urania Basin area, eastern Mediterranean.  
17 705 *Paleoceanography* 17(3). DOI: 10.1029/2000PA000536.  
18  
19  
20 706 D’Ortenzio F and D’Alcalà MR (2009) On the trophic regimes of the Mediterranean Sea: A satellite  
21  
22 707 analysis. *Biogeosciences* 6(2): 139–148. DOI: 10.5194/bg-6-139-2009.  
23  
24 708 Dansgaard W, Johnsen SJ, Clausen HB, et al. (1993) Evidence for general instability of the past  
25  
26 709 climate from a 250-kyr ice-core record. *Nature* 364: 218–220. DOI: 10.2307/1178566.  
27  
28  
29 710 Darling KF, Kucera M, Kroon D, et al. (2006) A resolution for the coiling direction paradox in  
30  
31 711 *Neogloboquadrina pachyderma*. *Paleoceanography* 21(2). John Wiley & Sons, Ltd: n/a-n/a.  
32 712 DOI: 10.1029/2005PA001189.  
33  
34  
35 713 De Lange GJ, Thomson J, Reitz A, et al. (2008) Synchronous basin-wide formation and redox-  
36  
37 714 controlled preservation of a Mediterranean sapropel. *Nature Geoscience* 1(9): 606–610. DOI:  
38 715 10.1038/ngeo283.  
39  
40  
41 716 De Rijk S, Troelstra SR and Rohling EJ (1999) Benthic foraminiferal distribution in the  
42  
43 717 Mediterranean Sea. *The Journal of Foraminiferal Research* 29(2). GeoScienceWorld: 93–103.  
44  
45 718 DOI: 10.2113/gsjfr.29.2.93.  
46  
47 719 Debret M, Bout-Roumazeilles V, Grousset F, et al. (2007) The origin of the 1500-year climate  
48  
49 720 cycles in Holocene North-Atlantic records. Available at: [https://hal-sde.archives-](https://hal-sde.archives-ouvertes.fr/hal-00330731/)  
50 721 [ouvertes.fr/hal-00330731/](https://hal-sde.archives-ouvertes.fr/hal-00330731/) (accessed 20 June 2019).  
52  
53  
54 722 Debret M, Sebag D, Crosta X, et al. (2009) Evidence from wavelet analysis for a mid-Holocene  
55 723 transition in global climate forcing. *Quaternary Science Reviews* 28(25–26). Elsevier Ltd:  
56 724 2675–2688. DOI: 10.1016/j.quascirev.2009.06.005.  
58  
59  
60 725 Desprat S, Combourieu-Nebout N, Essallami L, et al. (2013) Deglacial and holocene vegetation and  
726 climatic changes in the southern central Mediterranean from a direct land-sea correlation.



- 1  
2  
3 727 *Climate of the Past* 9(2): 767–787. DOI: 10.5194/cp-9-767-2013.  
4  
5  
6 728 Edelman-Furstenberg Y, Almogi-Labin A and Hemleben C (2009) Palaeoceanographic evolution of  
7  
8 729 the central Red Sea during the late Holocene. *Holocene* 19(1): 117–127. DOI:  
9 730 10.1177/0959683608098955.  
10  
11  
12 731 Fletcher WJ and Sánchez Goñi MF (2008) Orbital- and sub-orbital-scale climate impacts on  
13  
14 732 vegetation of the western Mediterranean basin over the last 48,000 yr. *Quaternary Research*  
15 733 70(3): 451–464. DOI: 10.1016/j.yqres.2008.07.002.  
16  
17  
18 734 Fletcher WJ, Debret M and Sanchez Goñi M (2012) The Holocene frequency millennial oscillation  
19  
20 735 in western Mediterranean climate: Implications for past dynamics of the North Atlantic  
21  
22 736 atmospheric westerlies. *The Holocene* 23(2): 153–166. DOI: 10.1177/0959683612460783.  
23  
24 737 Flores JA and Sierro FJ (1997) Revised technique for calculation of calcareous nannofossil  
25  
26 738 accumulation rates. *Micropaleontology* 43(3): 321–324. DOI: 10.2307/1485832.  
27  
28  
29 739 Flores JA, Gersonde RR, Sierro FJ, et al. (2000) Southern ocean pleistocene calcareous nannofossil  
30  
31 740 events: Calibration with isotope and geomagnetic stratigraphies. *Marine Micropaleontology*  
32 741 40(4): 377–402. DOI: 10.1016/S0377-8398(00)00047-5.  
33  
34  
35 742 Font J, Millot C, Salas J, et al. (1998) The drift of Modified Atlantic Water from the Alboran Sea to  
36  
37 743 the eastern Mediterranean. *Scientia Marina* 62(3): 211–216. DOI:  
38 744 10.3989/scimar.1998.62n3211.  
39  
40  
41 745 Font J, Puig P, Salat J, et al. (2007) Sequence of hydrographic changes in NW Mediterranean deep  
42  
43 746 water due to the exceptional winter of 2005. *Scientia Marina* 71(2): 339–346. DOI:  
44 747 10.3989/scimar.2007.71n2339.  
45  
46  
47 748 Foster G (1996) Wavelets for period analysis of unevenly sampled time series. *Astron. J.* 112:  
48 749 1709–1729.  
49  
50  
51  
52 750 Fraile I, Schulz M, Mulitza S, et al. (2008) Predicting the global distribution of planktonic  
53  
54 751 foraminifera using a dynamic ecosystem model. *Biogeosciences* 5: 891–911.  
55  
56 752 Frigola J, Moreno A, Cacho I, et al. (2007) Holocene climate variability in the western  
57  
58 753 Mediterranean region from a deepwater sediment record. *Paleoceanography* 22(2): 1–16. DOI:  
59 754 10.1029/2006PA001307.

- 1  
2  
3 755 Frigola J, Moreno A, Cacho I, et al. (2008) Evidence of abrupt changes in Western Mediterranean  
4  
5 756 Deep Water circulation during the last 50 kyr: A high-resolution marine record from the  
6  
7 757 Balearic Sea. *Quaternary International* 181(1): 88–104. DOI: 10.1016/j.quaint.2007.06.016.  
8  
9 758 Garcia-Gorriz E and Carr M-E (1999) The climatological annual cycle of satellite-derived  
10  
11 759 phytoplankton pigments in the Alboran sea. *Geophysical Research Letters* 26(19): 2985–2988.  
12  
13  
14 760 García Lafuente J, Fanjul EÁ, Vargas JM, et al. (2002) Subinertial variability in the flow through  
15  
16 761 the Strait of Gibraltar. *Journal of Geophysical Research* 107(C10). John Wiley & Sons, Ltd:  
17 762 3168. DOI: 10.1029/2001JC001104.  
18  
19  
20 763 García Lafuente J, Sánchez Román A, Díaz del Río G, et al. (2007) Recent observations of seasonal  
21  
22 764 variability of the Mediterranean outflow in the Strait of Gibraltar. *Journal of Geophysical*  
23  
24 765 *Research* 112(C10). John Wiley & Sons, Ltd: C10005. DOI: 10.1029/2006JC003992.  
25  
26 766 Gartner S, Chow J and Stanton RJ (1987) Late Neogene paleoceanography of the Eastern  
27  
28 767 Caribbean, the Gulf of Mexico, and the Eastern Equatorial Pacific. *Marine Micropaleontology*  
29  
30 768 12: 255–304.  
31  
32 769 Gimeno L, Nieto R, Trigo RM, et al. (2010) Where Does the Iberian Peninsula Moisture Come  
33  
34 770 From? An Answer Based on a Lagrangian Approach. *Journal of Hydrometeorology* 11(2):  
35  
36 771 421–436. DOI: 10.1175/2009JHM1182.1.  
37  
38  
39 772 Giraudeau J (1993) Planktonic foraminiferal assemblages in surface sediments from the southwest  
40  
41 773 African continental margin. *Marine Geology* 110(1–2). Elsevier: 47–62. DOI: 10.1016/0025-  
42 774 3227(93)90104-4.  
43  
44  
45 775 Giraudeau J, Pierre C and Herve L (2001) *A Late Quaternary, High-resolution Record Of*  
46  
47 776 *Planktonic Foraminiferal Species Distribution in The Southern Benguela Region: SITE 1087.*  
48 777 *Proceedings of the Ocean Drilling Program, Scientific Results.*  
49  
50  
51 778 Giraudeau J, Grelaud M, Solignac S, et al. (2010) Millennial-scale variability in Atlantic water  
52  
53 779 advection to the Nordic Seas derived from Holocene coccolith concentration records.  
54 780 *Quaternary Science Reviews* 29(9–10). Elsevier Ltd: 1276–1287. DOI:  
55  
56 781 10.1016/j.quascirev.2010.02.014.  
57  
58  
59 782 Girone A, Maiorano P, Marino M, et al. (2013) Calcareous plankton response to orbital and  
60  
783 millennial-scale climate changes across the Middle Pleistocene in the western Mediterranean.

- 1  
2  
3 784 *Palaeogeography, Palaeoclimatology, Palaeoecology* 392. Elsevier: 105–116. DOI:  
4  
5 785 10.1016/J.PALAEO.2013.09.005.  
6  
7  
8 786 Grelaud M, Beaufort L, Cuven S, et al. (2009) Glacial to interglacial primary production and El  
9 Niño-Southern Oscillation dynamics inferred from coccolithophores of the Santa Barbara  
10 Basin. *Paleoceanography* 24(1): 1–15. DOI: 10.1029/2007PA001578.  
11 788  
12  
13  
14 789 Hayes A, Kucera M, Kallel N, et al. (2005) Glacial Mediterranean sea surface temperatures based  
15 on planktonic foraminiferal assemblages. *Quaternary Science Reviews* 24(7–9). Pergamon:  
16 790 999–1016. DOI: 10.1016/J.QUASCIREV.2004.02.018.  
17 791  
18  
19  
20 792 Heburn GW and La Violette PE (1990) Variations in the structure of the anticyclonic gyres found in  
21 the Alboran Sea. *Journal of Geophysical Research* 95(C2): 1599. DOI:  
22 793 10.1029/JC095iC02p01599.  
23 794  
24  
25  
26 795 Hemleben C, Spindler M, Breiting I, et al. (1985) *Field and laboratory studies on the ontogeny*  
27 *and ecology of some globorotalid species from the Sargasso Sea off Bermuda. Journal of*  
28 796 *Foraminiferal Research*. v.  
29 797  
30  
31  
32 798 Hemleben C, Spindler M and Anderson OR (1989) Taxonomy and Species Features. In: *Modern*  
33 *Planktonic Foraminifera*. New York, NY: Springer New York, pp. 8–32. DOI: 10.1007/978-1-  
34 799 4612-3544-6\_2.  
35 800  
36  
37  
38 801 Hernández-Almeida I, Bárcena MA, Flores JA, et al. (2011) Microplankton response to  
39 802 environmental conditions in the Alboran Sea (Western Mediterranean): One year sediment trap  
40 803 record. *Marine Micropaleontology* 78(1–2). Elsevier: 14–24. DOI:  
41 804 10.1016/J.MARMICRO.2010.09.005.  
42  
43  
44  
45  
46 805 Hernández-Almeida I, Ausín B, Saavedra-Pellitero M, et al. (2019) Quantitative reconstruction of  
47 806 primary productivity in low latitudes during the last glacial maximum and the mid-to-late  
48 807 Holocene from a global Florisphaera profunda calibration dataset. *Quaternary Science Reviews*  
49 808 205: 166–181. DOI: 10.1016/J.QUASCIREV.2018.12.016.  
50  
51  
52  
53  
54 809 Howell MW and Thunell RC (1992) Organic carbon accumulation in Bannock Basin: Evaluating  
55 810 the role of productivity in the formation of eastern Mediterranean sapropels. *Marine Geology*  
56 811 103(1–3). Elsevier: 461–471. DOI: 10.1016/0025-3227(92)90032-D.  
57  
58  
59  
60 812 Huang NE, Shen Z, Long SR, et al. (1998) The empirical mode decomposition and Hilbert

- 1  
2  
3 813 spectrum for nonlinear and nonstationary time series analysis. *Proc. Roy. Soc. London A454*:  
4 903–995.  
5 814  
6  
7 815 Hurrell JW (1995) Decadal Trends in the North Atlantic Oscillation: Regional Temperatures and  
8 816 Precipitation. *Science* 269: 676–679.  
9  
10  
11  
12 817 Incarbona A, Sprovieri M, Di Stefano A, et al. (2013) Productivity modes in the mediterranean sea  
13 during dansgaard-oeschger (20,000-70,000yr ago) oscillations. *Palaeogeography,*  
14 818 *Palaeoclimatology, Palaeoecology* 392. Elsevier B.V.: 128–137. DOI:  
15 819 10.1016/j.palaeo.2013.09.023.  
16 820  
17 821 Jalali B, Sicre M-A, Bassetti MA, et al. (2016) Holocene climate variability in the North-Western  
18 822 Mediterranean Sea (Gulf of Lions). *Climate of the Past* 12(1): 91–101. DOI: 10.5194/cp-12-  
19 823 91-2016.  
20 824 Jalali B, Sicre M-A, Kallel N, et al. (2017) High-resolution Holocene climate and hydrological  
21 825 variability from two major Mediterranean deltas (Nile and Rhone). *Holocene* 27(8): 1158–  
22 826 1168. DOI: 10.1177/0959683616683258.  
23  
24  
25  
26 827 Jalut G, Esteban Amat A, Bonnet L, et al. (2000) Holocene climatic changes in the Western  
27 828 Mediterranean, from south-east France to south-east Spain. *Palaeogeography,*  
28 829 *Palaeoclimatology, Palaeoecology* 160(3–4): 255–290. DOI: 10.1016/S0031-0182(00)00075-  
29 830 4.  
30  
31  
32 831 Jalut G, Dedoubat JJ, Fontugne M, et al. (2009) Holocene circum-Mediterranean vegetation  
33 832 changes: Climate forcing and human impact. *Quaternary International* 200(1–2): 4–18. DOI:  
34 833 10.1016/j.quaint.2008.03.012.  
35  
36  
37  
38 834 Jiménez-Amat P and Zahn R (2015) Offset timing of climate oscillations during the last two glacial-  
39 835 interglacial transitions connected with large-scale freshwater perturbation. *Paleoceanography*  
40 836 30(6): 768–788. DOI: 10.1002/2014PA002710.  
41  
42  
43  
44 837 Jiménez-Espejo FJ, Martínez-Ruiz F, Sakamoto T, et al. (2007) Paleoenvironmental changes in the  
45 838 western Mediterranean since the last glacial maximum: High resolution multiproxy record  
46 839 from the Algero-Balearic basin. *Palaeogeography, Palaeoclimatology, Palaeoecology* 246(2–  
47 840 4): 292–306. DOI: 10.1016/j.palaeo.2006.10.005.  
48  
49  
50  
51  
52  
53 841 Jiménez-Espejo FJ, Martínez-Ruiz F, Rogerson M, et al. (2008) Detrital input, productivity

- 1  
2  
3 842 fluctuations, and water mass circulation in the westernmost Mediterranean Sea since the Last  
4  
5 843 Glacial Maximum. *Geochemistry, Geophysics, Geosystems* 9(11). DOI:  
6  
7 844 10.1029/2008GC002096.  
8  
9 845 Jonkers L, Brummer G-JA, C Peeters FJ, et al. (2010) Seasonal stratification, shell flux, and oxygen  
10  
11 846 isotope dynamics of left-coiling. *Paleoceanography* 25. DOI: 10.1029/2009PA001849.  
12  
13  
14 847 Jordan RW, Cros L and Young JR (2004) A revised classification scheme for living haptophytes.  
15  
16 848 *Micropaleontology* 50(Suppl\_1). GeoScienceWorld: 55–79. DOI: 10.2113/50.Suppl\_1.55.  
17  
18 849 Kallel N and Labeyrie L (1997) *Enhanced rainfall in the Mediterranean region during the last*  
19  
20 850 *Sapropel Event. Oceanologica Acta.*  
21  
22  
23 851 Kallel N, Duplessy J-C, Labeyrie L, et al. (2000) Mediterranean pluvial periods and sapropel  
24  
25 852 formation over the last 200 000 years. *Palaeogeography, Palaeoclimatology, Palaeoecology*  
26 853 157(1–2). Elsevier: 45–58. DOI: 10.1016/S0031-0182(99)00149-2.  
27  
28  
29 854 Knappertsbusch M (1993) Geographic distribution of living and Holocene coccolithophores in the  
30  
31 855 Mediterranean Sea. *Marine Micropaleontology* 21(1–3). Elsevier: 219–247. DOI:  
32 856 10.1016/0377-8398(93)90016-Q.  
33  
34  
35 857 Kontakiotis G (2016) Late Quaternary paleoenvironmental reconstruction and paleoclimatic  
36  
37 858 implications of the Aegean Sea (eastern Mediterranean) based on paleoceanographic indexes  
38  
39 859 and stable isotopes. *Quaternary International* 401. Elsevier Ltd: 28–42. DOI:  
40 860 10.1016/j.quaint.2015.07.039.  
41  
42  
43 861 Kucera M, Weinelt Mara, Kiefer T, et al. (2005) Reconstruction of sea-surface temperatures from  
44  
45 862 assemblages of planktonic foraminifera: Multi-technique approach based on geographically  
46 863 constrained calibration data sets and its application to glacial Atlantic and Pacific Oceans.  
47  
48 864 *Quaternary Science Reviews* 24(7-9 SPEC. ISS.). Pergamon: 951–998. DOI:  
49  
50 865 10.1016/j.quascirev.2004.07.014.  
51  
52  
53 866 Kutzbach JE, He F, Vavrus SJ, et al. (2013) The dependence of equilibrium climate sensitivity on  
54 867 climate state: Applications to studies of climates colder than present. *Geophysical Research*  
55  
56 868 *Letters* 40(14): 3721–3726. DOI: 10.1002/grl.50724.  
57  
58  
59 869 Lambeck K, Rouby H, Purcell A, et al. (2014) Sea level and global ice volumes from the Last  
60  
870 Glacial Maximum to the Holocene. *Proceedings of the National Academy of Sciences* 111(43):

- 1  
2  
3 871 15296–15303. DOI: 10.1073/pnas.1411762111.  
4  
5  
6 872 Laskar J, Robutel P, Joutel F, et al. (2004) A long-term numerical solution for the insolation  
7  
8 873 quantities of the Earth. *Astronomy & Astrophysics* 428(1). EDP Sciences: 261–285. DOI:  
9  
10 874 10.1051/0004-6361:20041335.  
11  
12 875 Lionello P (2012) *The Climate of the Mediterranean Region From the Past to the Future*. DOI:  
13  
14 876 10.1016/B978-0-12-416042-2.00009-4.  
15  
16  
17 877 Liqueste C, Arnau P, Canals M, et al. (2005) Mediterranean river systems of Andalusia, southern  
18 878 Spain, and associated deltas: A source to sink approach. *Marine Geology* 222–223(1–4): 471–  
19  
20 879 495. DOI: 10.1016/j.margeo.2005.06.033.  
21  
22  
23 880 Lirer F, Sprovieri M, Ferraro L, et al. (2013) Integrated stratigraphy for the Late Quaternary in the  
24  
25 881 eastern Tyrrhenian Sea. *Quaternary International* 292. Pergamon: 71–85. DOI:  
26 882 10.1016/J.QUAINT.2012.08.2055.  
27  
28  
29 883 Lobo FJ, Fernández-Salas LM, Moreno I, et al. (2006) The sea-floor morphology of a  
30  
31 884 Mediterranean shelf fed by small rivers, northern Alboran Sea margin. *Continental Shelf*  
32 885 *Research* 26(20). Pergamon: 2607–2628. DOI: 10.1016/j.csr.2006.08.006.  
33  
34  
35 886 Locarnini RA, Mishonov A V., Antonov JI, et al. (2013) World ocean atlas 2013. Volume 1,  
36  
37 887 Temperature. DOI: 10.7289/V55X26VD.  
38  
39  
40 888 Lomb NR (1976) Least-square frequency analysis of unequally spaced data. *Astrophys. Space Sci.*  
41 889 29: 447–462.  
42  
43  
44 890 Lowe JJ, Rasmussen SO, Björck S, et al. (2008) Synchronisation of palaeoenvironmental events in  
45  
46 891 the North Atlantic region during the Last Termination: a revised protocol recommended by the  
47 892 INTIMATE group. *Quaternary Science Reviews* 27(1–2): 6–17. DOI:  
48  
49 893 10.1016/j.quascirev.2007.09.016.  
50  
51  
52 894 Magny M, Miramont C and Sivan O (2002) Assessment of the impact of climate and anthropogenic  
53  
54 895 factors on Holocene Mediterranean vegetation in Europe on the basis of palaeohydrological  
55 896 records. *Palaeogeography, Palaeoclimatology, Palaeoecology* 186(1–2). Elsevier: 47–59.  
56  
57 897 DOI: 10.1016/S0031-0182(02)00442-X.  
58  
59  
60 898 Magny M, Combourieu-Nebout N, De Beaulieu JL, et al. (2013) North-south palaeohydrological  
899  
900 contrasts in the central mediterranean during the holocene: Tentative synthesis and working

1  
2  
3  
4  
5  
6  
7  
8  
9  
10  
11  
12  
13  
14  
15  
16  
17  
18  
19  
20  
21  
22  
23  
24  
25  
26  
27  
28  
29  
30  
31  
32  
33  
34  
35  
36  
37  
38  
39  
40  
41  
42  
43  
44  
45  
46  
47  
48  
49  
50  
51  
52  
53  
54  
55  
56  
57  
58  
59  
60  
928

hypotheses. *Climate of the Past* 9(5): 2043–2071. DOI: 10.5194/cp-9-2043-2013.

Margaritelli G, Vallefuoco M, Di Rita F, et al. (2016) Marine response to climate changes during the last five millennia in the central Mediterranean Sea. *Global and Planetary Change* 142. Elsevier: 53–72. DOI: 10.1016/J.GLOPLACHA.2016.04.007.

Marino M, Maiorano P, Tarantino F, et al. (2014) Coccolithophores as proxy of seawater changes at orbital-to-millennial scale during middle Pleistocene Marine Isotope Stages 14-9 in North Atlantic core MD01-2446. *Paleoceanography* 29(6). John Wiley & Sons, Ltd: 518–532. DOI: 10.1002/2013PA002574.

Martrat B, Grimalt JO, Lopez-Martinez C, et al. (2004) Abrupt temperature changes in the Western Mediterranean over the past 250,000 years. *Science (New York, N.Y.)* 306(5702). American Association for the Advancement of Science: 1762–5. DOI: 10.1126/science.1101706.

Martrat B, Jimenez-Amat P, Zahn R, et al. (2014) Similarities and dissimilarities between the last two deglaciations and interglaciations in the North Atlantic region. *Quaternary Science Reviews* 99(October 2016): 122–134. DOI: 10.1016/j.quascirev.2014.06.016.

Mayewski PA, Rohling EJ, Stager CJ, et al. (2004) Holocene climate variability. *Quaternary Research* 62: 243–255. DOI: 10.1016/j.yqres.2004.07.001.

Meijer PT and Tuenter E (2007) The effect of precession-induced changes in the Mediterranean freshwater budget on circulation at shallow and intermediate depth. *Journal of Marine Systems* 68(3–4). Elsevier: 349–365. DOI: 10.1016/J.JMARSYS.2007.01.006.

Mertens C and Schott F (1998) Interannual Variability of Deep-Water Formation in the Northwestern Mediterranean. *journal of physical oceanography* 28: 1410–1428.

Millot C (2008) Short-term variability of the Mediterranean in- and out-flows. *Geophysical Research Letters* 35(15). John Wiley & Sons, Ltd: L15603. DOI: 10.1029/2008GL033762.

Moreno A, Cacho I, Canals M, et al. (2004) Millennial-scale variability in the productivity signal from the Alboran Sea record, Western Mediterranean Sea. *Palaeogeography, Palaeoclimatology, Palaeoecology* 211(3–4). Elsevier: 205–219. DOI: 10.1016/J.PALAEO.2004.05.007.

Moreno A, Cacho I, Canals M, et al. (2005) Links between marine and atmospheric processes oscillating on a millennial time-scale. A multi-proxy study of the last 50,000 yr from the

- 1  
2  
3 929 Alboran Sea (Western Mediterranean Sea). *Quaternary Science Reviews* 24(14–15): 1623–  
4 1636. DOI: 10.1016/j.quascirev.2004.06.018.  
5 930  
6  
7  
8 931 Moreno A, Pérez A, Frigola J, et al. (2012) The Medieval Climate Anomaly in the Iberian  
9 Peninsula reconstructed from marine and lake records. *Quaternary Science Reviews* 43.  
10 Elsevier Ltd: 16–32. DOI: 10.1016/j.quascirev.2012.04.007.  
11 933  
12  
13  
14 934 Moreno E, Thouveny N, Delanghe D, et al. (2002) Climatic and oceanographic changes in the  
15 Northeast Atlantic reflected by magnetic properties of sediments deposited on the Portuguese  
16 Margin during the last 340 ka. *Earth and Planetary Science Letters* 202(2). Elsevier: 465–480.  
17 936  
18 DOI: 10.1016/S0012-821X(02)00787-2.  
19 937  
20  
21  
22 938 Munz PM, Siccha M, Lückge A, et al. (2015) Decadal-resolution record of winter monsoon  
23 intensity over the last two millennia from planktic foraminiferal assemblages in the  
24 northeastern Arabian Sea. *Holocene* 25(11). SAGE Publications Ltd: 1756–1771. DOI:  
25 940  
26 10.1177/0959683615591357.  
27 941  
28  
29  
30 942 Nieto-Moreno V, Martínez-Ruiz F, Giral S, et al. (2011) Tracking climate variability in the western  
31 Mediterranean during the Late Holocene: A multiproxy approach. *Climate of the Past* 7(4):  
32 1395–1414. DOI: 10.5194/cp-7-1395-2011.  
33 944  
34  
35  
36 945 Nieto-Moreno V, Martínez-Ruiz F, Gallego-Torres D, et al. (2015) Palaeoclimate and  
37 palaeoceanographic conditions in the westernmost Mediterranean over the last millennium: an  
38 integrated organic and inorganic approach. *Journal of the Geological Society* 172(2): 264–271.  
39 947  
40 DOI: 10.1144/jgs2013-105.  
41 948  
42  
43  
44 949 Okada H and Wells P (1997) Late Quaternary nannofossil indicators of climate change in two deep-  
45 sea cores associated with the Leeuwin Current off Western Australia. *Palaeogeography,*  
46 *Palaeoclimatology, Palaeoecology* 131(3–4). Elsevier: 413–432. DOI: 10.1016/S0031-  
47 951  
48 0182(97)00014-X.  
49 952  
50  
51  
52 953 Olsen J, Anderson NJ and Knudsen MF (2012) Variability of the North Atlantic Oscillation over  
53 the past 5,200 years. *Nature Geoscience* 5(11): 808–812. DOI: 10.1038/ngeo1589.  
54 954  
55  
56 955 Oviedo AM, Ziveri P and Gazeau F (2017) Coccolithophore community response to increasing  
57 pCO<sub>2</sub> in Mediterranean oligotrophic waters. *Estuarine, Coastal and Shelf Science* 186: 58–71.  
58 956  
59 DOI: 10.1016/j.ecss.2015.12.007.  
60 957



- 1  
2  
3 958 Pérez-Folgado M, Sierro FJ, Flores JA, et al. (2003) Western Mediterranean planktonic  
4  
5 959 foraminifera events and millennial climatic variability during the last 70 kyr. *Marine*  
6  
7 960 *Micropaleontology* 48(1–2). Elsevier: 49–70. DOI: 10.1016/S0377-8398(02)00160-3.  
8  
9 961 Pérez-Folgado M, Sierro FJ, Flores JA, et al. (2004) Paleoclimatic variations in foraminifer  
10  
11 962 assemblages from the Alboran Sea (Western Mediterranean) during the last 150 ka in ODP  
12  
13 963 Site 977. *Marine Geology* 212(1–4): 113–131. DOI: 10.1016/j.margeo.2004.08.002.  
14  
15 964 Perkins H, Kinder T and La Violette PE (1990) The Atlantic Inflow in the Western Alboran Sea.  
16  
17 965 *Journal of Physical Oceanography* 20: 242–263.  
18  
19  
20 966 Peyron O, Combourieu-Nebout N, Brayshaw D, et al. (2017) Precipitation changes in the  
21  
22 967 Mediterranean basin during the Holocene from terrestrial and marine pollen records: A model-  
23  
24 968 data comparison. *Climate of the Past* 13(3): 249–265. DOI: 10.5194/cp-13-249-2017.  
25  
26 969 Pflaumann U, Duprat J, Pujol C, et al. (1996) SIMMAX: A modern analog technique to deduce  
27  
28 970 Atlantic sea surface temperatures from planktonic foraminifera in deep-sea sediments.  
29  
30 971 *Paleoceanography* 11(1). John Wiley & Sons, Ltd: 15–35. DOI: 10.1029/95PA01743.  
31  
32 972 Piva A, Asioli A, Andersen N, et al. (2008) Climatic cycles as expressed in sediments of the  
33  
34 973 PROMESS1 borehole PRAD1-2, central Adriatic, for the last 370 ka: 2. Paleoenvironmental  
35  
36 974 evolution. *Geochemistry, Geophysics, Geosystems* 9(3). John Wiley & Sons, Ltd: n/a-n/a. DOI:  
37  
38 975 10.1029/2007GC001785.  
39  
40 976 Principato MS, Crudeli D, Ziveri P, et al. (2006) Phyto\_ and zooplankton paleofluxes during the  
41  
42 977 deposition of sapropel S1 (eastern Mediterranean): Biogenic carbonate preservation and  
43  
44 978 paleoecological implications. *Palaeogeography, Palaeoclimatology, Palaeoecology* 235(1–3).  
45  
46 979 Elsevier: 8–27. DOI: 10.1016/J.PALAEO.2005.09.021.  
47  
48 980 Pujol C and Vergnaud-Grazzini C (1995) Distribution patterns of live planktic foraminifers as  
49  
50 981 related to regional hydrography and productive systems of the Mediterranean Sea. *Marine*  
51  
52 982 *Micropaleontology* 25(2–3). Elsevier: 187–217. DOI: 10.1016/0377-8398(95)00002-I.  
53  
54 983 Ramos-Román MJ, Jiménez-Moreno G, Camuera J, et al. (2018) Millennial-scale cyclical  
55  
56 984 environment and climate variability during the Holocene in the western Mediterranean region  
57  
58 985 deduced from a new multi-proxy analysis from the Padul record (Sierra Nevada, Spain).  
59  
60 986 *Global and Planetary Change* 168(June). Elsevier: 35–53. DOI:  
987 10.1016/j.gloplacha.2018.06.003.

- 1  
2  
3 988 Rasmussen SO, Andersen KK, Svensson AM, et al. (2006) A new Greenland ice core chronology  
4 for the last glacial termination. *Journal of Geophysical Research Atmospheres* 111(6): 1–16.  
5 989 DOI: 10.1029/2005JD006079.  
6 990  
7  
8  
9 991 Repschläger J, Garbe-Schönberg D, Weinelt M, et al. (2017) Holocene evolution of the North  
10 Atlantic subsurface transport. *Climate of the Past* 13(4): 333–344. DOI: 10.5194/cp-13-333-  
11 992 2017.  
12 993  
13  
14  
15 994 Rigual-Hernández AS, Sierro FJ, Bárcena MA, et al. (2012) Seasonal and interannual changes of  
16 planktic foraminiferal fluxes in the Gulf of Lions (NW Mediterranean) and their implications  
17 995 for paleoceanographic studies: Two 12-year sediment trap records. *Deep Sea Research Part I:  
18 Oceanographic Research Papers* 66. Pergamon: 26–40. DOI: 10.1016/J.DSR.2012.03.011.  
19 996  
20 997  
21  
22  
23 998 Rixen M, Beckers JM, Levitus S, et al. (2005) The Western Mediterranean Deep Water: A proxy  
24 for climate change. *Geophysical Research Letters* 32(12): 1–4. DOI: 10.1029/2005GL022702.  
25 999  
26  
27  
28 1000 Rodrigo-Gámiz M, Martínez-Ruiz F, Jiménez-Espejo FJ, et al. (2011) Impact of climate variability  
29 in the western Mediterranean during the last 20,000 years: Oceanic and atmospheric responses.  
30 1001 *Quaternary Science Reviews* 30(15–16). Elsevier Ltd: 2018–2034. DOI:  
31 1002 10.1016/j.quascirev.2011.05.011.  
32 1003  
33  
34  
35 1004 Rogerson M, Cacho I, Jimenez-Espejo FJ, et al. (2008) A dynamic explanation for the origin of the  
36 western Mediterranean organic-rich layers. *Geochemistry, Geophysics, Geosystems* 9(7). John  
37 1005 Wiley & Sons, Ltd: n/a-n/a. DOI: 10.1029/2007GC001936.  
38 1006  
39  
40  
41  
42 1007 Rohling EJ and Pälike H (2005) Centennial-scale climate cooling with a sudden cold event around  
43 8,200 years ago. *Nature* 434(7036): 975–979. DOI: 10.1038/nature03421.  
44 1008  
45  
46 1009 Rohling EJ, Den Dulk M, Pujol C, et al. (1995) Abrupt hydrographic change in the Alboran Sea  
47 (western Mediterranean) around 8000 yrs BP. *Deep-Sea Research Part I* 42(9): 1609–1619.  
48 1010 DOI: 10.1016/0967-0637(95)00069-I.  
49 1011  
50  
51  
52 1012 Rohling EJ, Jorissen FJ and De Stigter HC (1997) 200 Year interruption of Holocene sapropel  
53 formation in the Adriatic Sea. *Journal of Micropalaeontology* 16(2): 97–108. DOI:  
54 1013 10.1144/jm.16.2.97.  
55 1014  
56  
57  
58 1015 Rohling EJ, Cane TR, Cooke S, et al. (2002) African monsoon variability during the previous  
59 interglacial maximum. *Earth and Planetary Science Letters* 202(1). Elsevier: 61–75. DOI:  
60 1016

1

2

3 1017 10.1016/S0012-821X(02)00775-6.

4

5

6 1018 Rohling EJ, Sprovieri M, Cane T, et al. (2004) Reconstructing past planktic foraminiferal habitats

7

8 1019 using stable isotope data: a case history for Mediterranean sapropel S5. *Marine*

9

10 1020 *Micropaleontology* 50(1–2). Elsevier: 89–123. DOI: 10.1016/S0377-8398(03)00068-9.

11

12 1021 Rohling EJ, Marino G and Grant KM (2015) Mediterranean climate and oceanography, and the

13

14 1022 periodic development of anoxic events (sapropels). *Earth-Science Reviews* 143. Elsevier B.V.:

15

16 1023 62–97. DOI: 10.1016/j.earscirev.2015.01.008.

17

18 1024 Rossignol-Strick M (1985) Mediterranean Quaternary sapropels, an immediate response of the

19

20 1025 African monsoon to variation of insolation. *Palaeogeography, Palaeoclimatology,*

21

22 1026 *Palaeoecology* 49(3–4). Elsevier: 237–263. DOI: 10.1016/0031-0182(85)90056-2.

23

24 1027 Rossignol-Strick M, Nesteroff W, Olive P, et al. (1982) After the deluge: Mediterranean stagnation

25

26 1028 and sapropel formation. *Nature* 295(5845). Nature Publishing Group: 105–110. DOI:

27

28 1029 10.1038/295105a0.

29

30 1030 Salgueiro E, Voelker AHL, de Abreu L, et al. (2010) Temperature and productivity changes off the

31

32 1031 western Iberian margin during the last 150 ky. *Quaternary Science Reviews* 29(5–6).

33

34 1032 Pergamon: 680–695. DOI: 10.1016/J.QUASCIREV.2009.11.013.

35

36 1033 Salgueiro E, Naughton F, Voelker AHL, et al. (2014) Past circulation along the western Iberian

37

38 1034 margin: A time slice vision from the Last Glacial to the Holocene. *Quaternary Science*

39

40 1035 *Reviews* 106: 316–329. DOI: 10.1016/j.quascirev.2014.09.001.

41

42 1036 Sarhan T, García-Lafuente J, Vargas M, et al. (2000) Upwelling mechanisms in the northwestern

43

44 1037 Alboran Sea. *Journal of Marine Systems* 23(4): 317–331. DOI: 10.1016/S0924-

45

46 1038 7963(99)00068-8.

47

48 1039 Sbaffi L, Wezel FC, Kallel N, et al. (2001) Response of the pelagic environment to palaeoclimatic

49

50 1040 changes in the central Mediterranean Sea during the Late Quaternary. *Marine Geology* 178(1–

51

52 1041 4): 39–62. DOI: 10.1016/S0025-3227(01)00185-2.

53

54 1042 Scargle JD (1982) Studies in astronomical time series analysis, II Statistical aspects of spectral

55

56 1043 analysis of unevenly spaced data. *Astrophys. J.* 263: 835–853.

57

58 1044 Schiebel R, Waniek J, Bork M, et al. (2001) Planktic foraminiferal production stimulated by

59

60 1045 chlorophyll redistribution and entrainment of nutrients. *Deep Sea Research Part I:*

- 1  
2  
3 1046 *Oceanographic Research Papers* 48(3). Pergamon: 721–740. DOI: 10.1016/S0967-  
4 0637(00)00065-0.  
5 1047  
6  
7  
8 1048 Schirmacher J, Weinelt M, Blanz T, et al. (2019) Multi-decadal climate variability in southern  
9 Iberia during the mid- to late-Holocene. *Climate of the Past Discussions*: 1–29. DOI:  
10 1049 10.5194/cp-2018-158.  
11 1050  
12  
13  
14 1051 Schulz M and Mudelsee M (2002) REDFIT: estimating red-noise spectra directly from unevenly  
15 spaced paleoclimatic time series. *Comput. Geosci.* 28: 421–426.  
16 1052  
17  
18 1053 Siccha M, Trommer G, Schulz H, et al. (2009) Factors controlling the distribution of planktonic  
19 foraminifera in the Red Sea and implications for the development of transfer functions. *Marine*  
20 1054 *Micropaleontology* 72(3–4). Elsevier: 146–156. DOI: 10.1016/J.MARMICRO.2009.04.002.  
21 1055  
22  
23  
24 1056 Sierro FJ, Hodell DA, Curtis JH, et al. (2005) Impact of iceberg melting on Mediterranean  
25 thermohaline circulation during Heinrich events. *Paleoceanography* 20(2): 1–13. DOI:  
26 1057 10.1029/2004PA001051.  
27 1058  
28  
29  
30 1059 Smith AC, Wynn PM, Barker PA, et al. (2016) North Atlantic forcing of moisture delivery to  
31 Europe throughout the Holocene. *Scientific Reports* 6. Nature Publishing Group: 1–7. DOI:  
32 1060 10.1038/srep24745.  
33 1061  
34  
35  
36 1062 Smith RO, Bryden HL and Stansfield K (2008) *Observations of new western Mediterranean deep*  
37 *water formation using Argo floats.* *Ocean Sci.*  
38 1063  
39  
40  
41 1064 Spezzaferri S, Kucera M, Pearson PN, et al. (2015) Fossil and Genetic Evidence for the  
42 Polyphyletic Nature of the Planktonic Foraminifera ‘Globigerinoides’, and Description of the  
43 1065 New Genus *Trilobatus*. Abramovich S (ed.) *PLOS ONE* 10(5). Public Library of Science. DOI:  
44 1066 10.1371/journal.pone.0128108.  
45 1067  
46  
47  
48  
49 1068 Sprovieri M, Di Stefano E, Incarbona A, et al. (2012) Centennial- to millennial-scale climate  
50 oscillations in the Central-Eastern Mediterranean Sea between 20,000 and 70,000 years ago:  
51 1069 Evidence from a high-resolution geochemical and micropaleontological record. *Quaternary*  
52 1070 *Science Reviews* 46: 126–135. DOI: 10.1016/j.quascirev.2012.05.005.  
53 1071  
54  
55  
56  
57 1072 Sprovieri R, Di Stefano E, Incarbona A, et al. (2003) A high-resolution record of the last  
58 deglaciation in the Sicily Channel based on foraminifera and calcareous nannofossil  
59 1073 quantitative distribution. *Palaeogeography, Palaeoclimatology, Palaeoecology* 202(1–2): 119–  
60 1074

- 1  
2  
3 1075 142. DOI: 10.1016/S0031-0182(03)00632-1.  
4  
5  
6 1076 Steinmetz JC (1994) Sedimentation of Coccolithophores. In: *Coccolithophores*, pp. 179–183.  
7  
8  
9 1077 Stolz K and Baumann K-H (2010) Changes in palaeoceanography and palaeoecology during  
10  
11 1078 Marine Isotope Stage (MIS) 5 in the eastern North Atlantic (ODP Site 980) deduced from  
12 1079 calcareous nannoplankton observations. *Palaeogeography, Palaeoclimatology, Palaeoecology*  
13  
14 1080 292(1–2). Elsevier B.V.: 295–305. DOI: 10.1016/j.palaeo.2010.04.002.  
15  
16  
17 1081 Sumner G, Homar V and Ramis C (2001) Precipitation seasonality in eastern and southern coastal  
18 1082 Spain. *International Journal of Climatology* 21(2). John Wiley & Sons, Ltd: 219–247. DOI:  
19  
20 1083 10.1002/joc.600.  
21  
22  
23 1084 Takahashi K and Okada H (2000) Environmental control on the biogeography of modern  
24 1085 coccolithophores in the southeastern Indian Ocean offshore of Western Australia. *Marine*  
25  
26 1086 *Micropaleontology* 39(1–4): 73–86. DOI: 10.1016/S0377-8398(00)00015-3.  
27  
28  
29 1087 Thornalley DJR, Elderfield H and McCave N (2009) Holocene oscillations in temperature and  
30  
31 1088 salinity of the surface subpolar North Atlantic. *Nature* 457. Nature Publishing Group: 711–  
32  
33 1089 713. DOI: 10.1038/nature07717.  
34  
35 1090 Toucanne S, Zaragosi S, Bourillet J-F, et al. (2012) External controls on turbidite sedimentation on  
36  
37 1091 the glacially-influenced Armorican margin (Bay of Biscay, western European margin). *Marine*  
38  
39 1092 *Geology* 303–306. Elsevier: 137–153. DOI: 10.1016/J.MARGEO.2012.02.008.  
40  
41 1093 Toucanne S, Angue Minto'o CM, Fontanier C, et al. (2015) Tracking rainfall in the northern  
42  
43 1094 Mediterranean borderlands during sapropel deposition. *Quaternary Science Reviews* 129.  
44  
45 1095 Pergamon: 178–195. DOI: 10.1016/J.QUASCIREV.2015.10.016.  
46  
47 1096 Triantaphyllou M, Antonarakou A, Dimiza M, et al. (2010) Calcareous nannofossil and planktonic  
48  
49 1097 foraminiferal distributional patterns during deposition of sapropels S6, S5 and S1 in the Libyan  
50  
51 1098 Sea (Eastern Mediterranean). *Geo-Marine Letters* 30(1): 1–13. DOI: 10.1007/s00367-009-  
52  
53 1099 0145-7.  
54  
55 1100 Trigo R, Pozo-Vázquez D, Osborn TJ, et al. (2004) North Atlantic oscillation influence on  
56  
57 1101 precipitation, river flow and water resources in the Iberian Peninsula. *International Journal of*  
58  
59 1102 *Climatology* 24(8): 925–944. DOI: 10.1002/joc.1048.  
60  
1103 Tzedakis PC (2007) Seven ambiguities in the Mediterranean palaeoenvironmental narrative.

- 1  
2  
3 1104 *Quaternary Science Reviews* 26(17–18). Pergamon: 2042–2066. DOI:  
4  
5 1105 10.1016/J.QUASCIREV.2007.03.014.  
6  
7  
8 1106 Vallefucio M, Lirer F, Ferraro L, et al. (2012) Climatic variability and anthropogenic signatures in  
9  
10 1107 the Gulf of Salerno (southern-eastern Tyrrhenian Sea) during the last half millennium.  
11 1108 *Rendiconti Lincei* 23(1). Springer Milan: 13–23. DOI: 10.1007/s12210-011-0154-0.  
12  
13  
14 1109 Vargas-Yáñez M, Jesús García M, Salat J, et al. (2008) Warming trends and decadal variability in  
15  
16 1110 the Western Mediterranean shelf. *Global and Planetary Change* 63(2–3). Elsevier: 177–184.  
17 1111 DOI: 10.1016/J.GLOPLACHA.2007.09.001.  
18  
19  
20 1112 Vincent E and Berger WH (1981) Planktonic foraminifera and their use in paleoceanography. *The*  
21  
22 1113 *Sea* 7: 371–412.  
23  
24  
25 1114 Viúdez Á, Tintoré J, Haney RL, et al. (1996) Circulation in the Alboran Sea as Determined by  
26 1115 Quasi-Synoptic Hydrographic Observations. Part I: Three-Dimensional Structure of the Two  
27  
28 1116 Anticyclonic Gyres. *Journal of Physical Oceanography* 26(5): 684–705. DOI: 10.1175/1520-  
29  
30 1117 0485(1996)026<0684:CITASA>2.0.CO;2.  
31  
32  
33 1118 Walker MJC, Berkelhammer M, Björck S, et al. (2012) Formal subdivision of the Holocene  
34 1119 Series/Epoch: A Discussion Paper by a Working Group of INTIMATE (Integration of ice-  
35  
36 1120 core, marine and terrestrial records) and the Subcommittee on Quaternary Stratigraphy  
37  
38 1121 (International Commission on Stratigraphy). *Journal of Quaternary Science* 27(7): 649–659.  
39 1122 DOI: 10.1002/jqs.2565.  
40  
41  
42 1123 Wanner H, Mercolli L, Grosjean M, et al. (2015) Holocene climate variability and change; a data-  
43  
44 1124 based review. *Journal of the Geological Society* 172(2): 254–263. DOI: 10.1144/jgs2013-101.  
45  
46  
47 1125 Weaver PPE and Pujol C (1988) History of the last deglaciation in the alboran sea (western  
48 1126 Mediterranean) and adjacent north Atlantic as revealed by coccolith floras. *Palaeogeography,*  
49  
50 1127 *Palaeoclimatology, Palaeoecology* 64(1–2): 35–42. DOI: 10.1016/0031-0182(88)90140-X.  
51  
52  
53 1128 Winter A and Siesser WG (1994) *Coccolithophores*. Cambridge University Press.  
54  
55  
56 1129 Young J, Geisen M, Cros L, et al. (2003) A guide to extant coccolithophore taxonomy. *Journal of*  
57 1130 *Nannoplankton Research Special Issue* 1.  
58  
59  
60 1131 Zachariasse W-J, Jorissen FJ, Perissoratis C, et al. (1997) Late Quaternary foraminiferal changes  
1132 and the nature of Sapropel S1 in Skopelos Basin. *Proceeding of the 5th Hellenic Symposium*

1  
2  
3 1133 on *Oceanography and Fisheries* 1: 391–394.  
4

5  
6 1134 Zanchetta G, Drysdale RN, Hellstrom JC, et al. (2007) Enhanced rainfall in the Western  
7  
8 1135 Mediterranean during deposition of sapropel S1: stalagmite evidence from Corchia cave  
9  
10 1136 (Central Italy). *Quaternary Science Reviews* 26(3–4): 279–286. DOI:  
11 1137 10.1016/j.quascirev.2006.12.003.  
12

13  
14 138 Zielhofer C, Fletcher WJ, Mischke S, et al. (2017) Atlantic forcing of Western Mediterranean  
15  
16 139 winter rain minima during the last 12,000 years. *Quaternary Science Reviews* 157. Elsevier  
17 140 Ltd: 29–51. DOI: 10.1016/j.quascirev.2016.11.037.  
18  
19

20 141  
21  
22  
23 142 **Figure captions**  
24

25 143  
26 144 *Fig. 1:* Location of ODP Site 976 in the Alboran Sea (western Mediterranean), bathymetry of the  
27  
28 145 area and modern-day oceanographic circulation. **AW** (Atlantic Water); **MOW** (Mediterranean  
29  
30 146 Outflow Water); **WMDW** (western Mediterranean Deep Water); **LIW** (Levantine Intermediate  
31 147 Water); **WAG** (western Alboran Gyre); **EAG** (eastern Alboran Gyre). In violet shade: Alboran and  
32  
33 148 Almeria-Oran upwelling fronts  
34  
35 149

36 150 *Fig. 2:* Downcore variations of calcareous nannofossil assemblages at Site 976 plotted as relative  
37  
38 151 abundance (%; black line) and nannofossil accumulation rate - NAR (coccolith/cm<sup>2</sup> kyr, filled area).  
39  
40 152 Sedimentation rate over time used for NAR calculation, from Martrat et al. (2014), is also shown.  
41  
42 153 YD: Younger Dryas.  
43

44 154  
45 155 *Fig. 3:* Downcore variations of planktonic foraminifera assemblages at Site 976 plotted as relative  
46  
47 156 abundance (%; black line) and planktonic foraminifera accumulation rate – pfAR (forams/cm<sup>2</sup>kyr,  
48  
49 157 filled area), together with foraminifera-based summer, winter and annual SST and similarity index.  
50  
51 158 Sedimentation rate over time, used for pfAR calculation, from Martrat et al. (2014). YD: Younger  
52 159 Dryas.  
53

54 160  
55 161 *Fig. 4:*(a) Signal of the Total NAR decomposed with CEEMD in five IMFs plus a residue (trend);  
56  
57 162 (b), (c), (d), (e) spectral analysis made with “REDFIT” and Foster’s WWZ, of the IMFs extracted  
58  
59 163 from Total NAR. The green and black line represent the 95% and 80% Confident Level  
60  
1164 respectively. Significantly periodicity (red dot) and relative values expressed in years were

1  
2  
3 1165 reported.

4  
5 1166

6  
7 1167 *Fig. 5: Abundances variations of calcareous plankton assemblage and additional proxies from Site*  
8 1168 *976: accumulation rate of selected coccolithophores and planktonic foraminifera; relative*  
9 1169 *abundance patterns of selected pollen taxa at Site 976 from Combourieu-Nebout et al. (2009); black*  
10 1170 *line, 3 point average. Di- and tri-unsaturated alkenones of 37 carbons (C<sub>37</sub>) from Martrat et al.*  
11 1171 *(2014) and summer insolation curve (Laskar et al., 2004) are also shown. Younger Dryas (YD, grey*  
12 1172 *bar); 8.2 ka event (light blue bar); dashed black lines are used to trace boundaries among phases I-*  
13 1173 *III.*

14  
15 1174

16  
17 1175 *Fig. 6: Abundances variations of calcareous plankton assemblage and additional proxies from Site*  
18 1176 *976: accumulation rate of selected coccolithophores and planktonic foraminifera; black line, 3 point*  
19 1177 *average; foram based seasonal SST variations at Site 976; relative abundance patterns of selected*  
20 1178 *pollen taxa at Site 976 from Combourieu-Nebout et al. (2009). 8.2 ka event (dotted bar),*  
21 1179 *dashed black lines are used to trace boundaries among phases I-III.*

22  
23 1180

24 1181 *Fig. 7: Abundances variation of coccolithophore assemblage and climate proxies from Site 976: *G.**  
25 1182 **oceanica* absolute abundances (black line, 3 point average);  $\delta^{18}\text{O}_{\text{seawater}}$  at Site 976 (green line, 3*  
26 1183 *point average) (Jimenez-Amat and Zahn, 2015);  $\delta^{18}\text{O}$  of combined and de-trended speleothems*  
27 1184 *from Iberian Peninsula (Smith et al., 2016); coccolithophore productivity (total Nannofossil*  
28 1185 *Accumulation Rate) at Site 976 (black line, 3 point average). Inferred NAO circulation pattern from*  
29 1186 *redox variability from Lake SS1220, Greenland (Olsen et al., 2012) is also shown. Light blue bars*  
30 1187 *represent periods of increased total NAR concomitant with enhanced Atlantic inflow and positive*  
31 1188 *NAO index phases.*

32  
33 1189

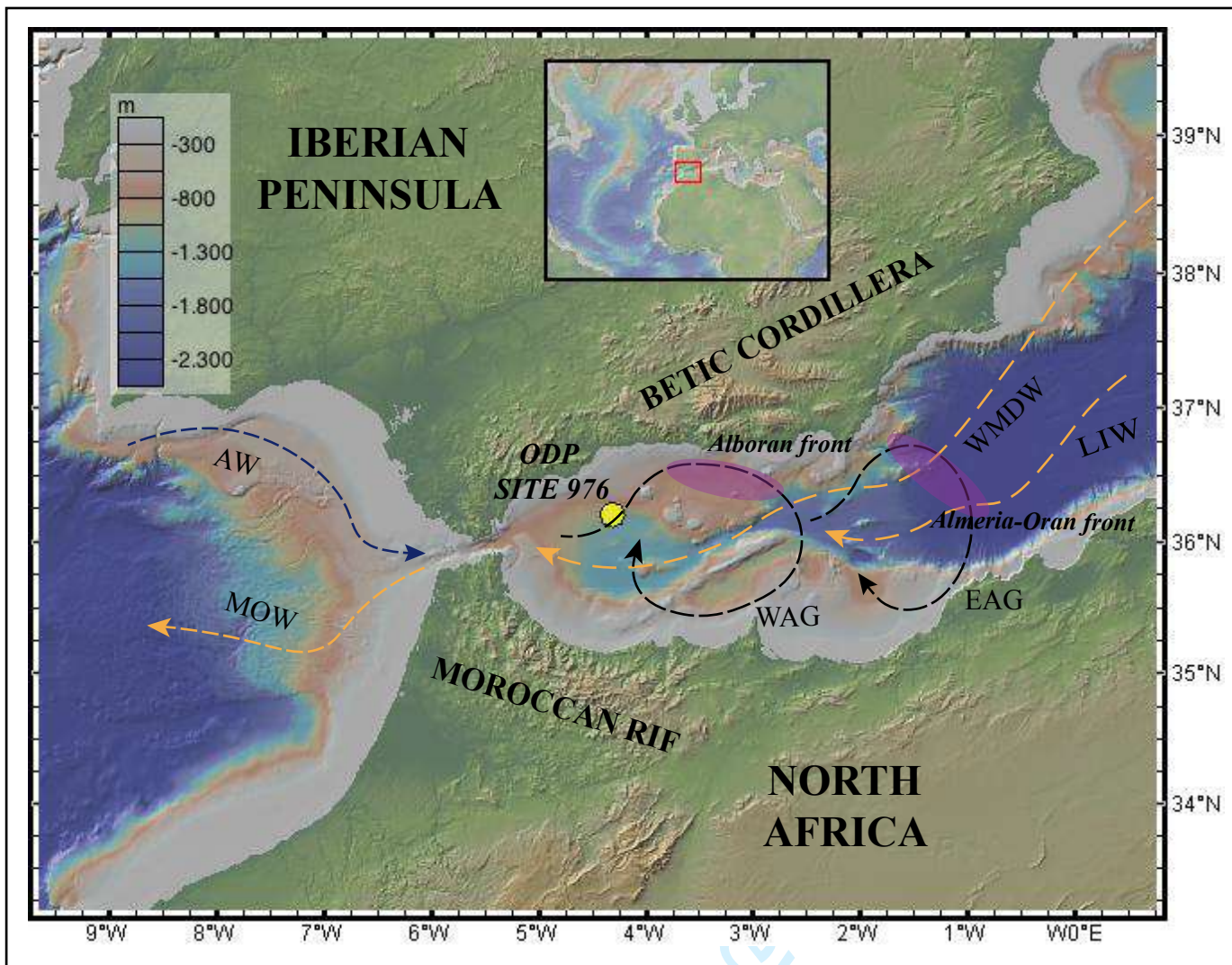
34 1190 *Fig. 8: Proposed different NAO circulations pattern scenarios as explained in the text: a) **NAO+***  
35 1191 *enhanced northwesterly winds, deep water formation and Atlantic inflow inducing upwelling and*  
36 1192 *coccolithophore productivity; b) **NAO-** reduced northwesterly winds, deep water formation and*  
37 1193 *Atlantic inflow, inducing stratification and reduced coccolithophore productivity. **LIW** (Levantine*  
38 1194 *Intermediate Water). **AJ** (Atlantic Jet); **WMDW** (western Mediterranean Deep Water). **MOW***  
39 1195 *(Mediterranean Outflow Water). Diagram not to scale.*

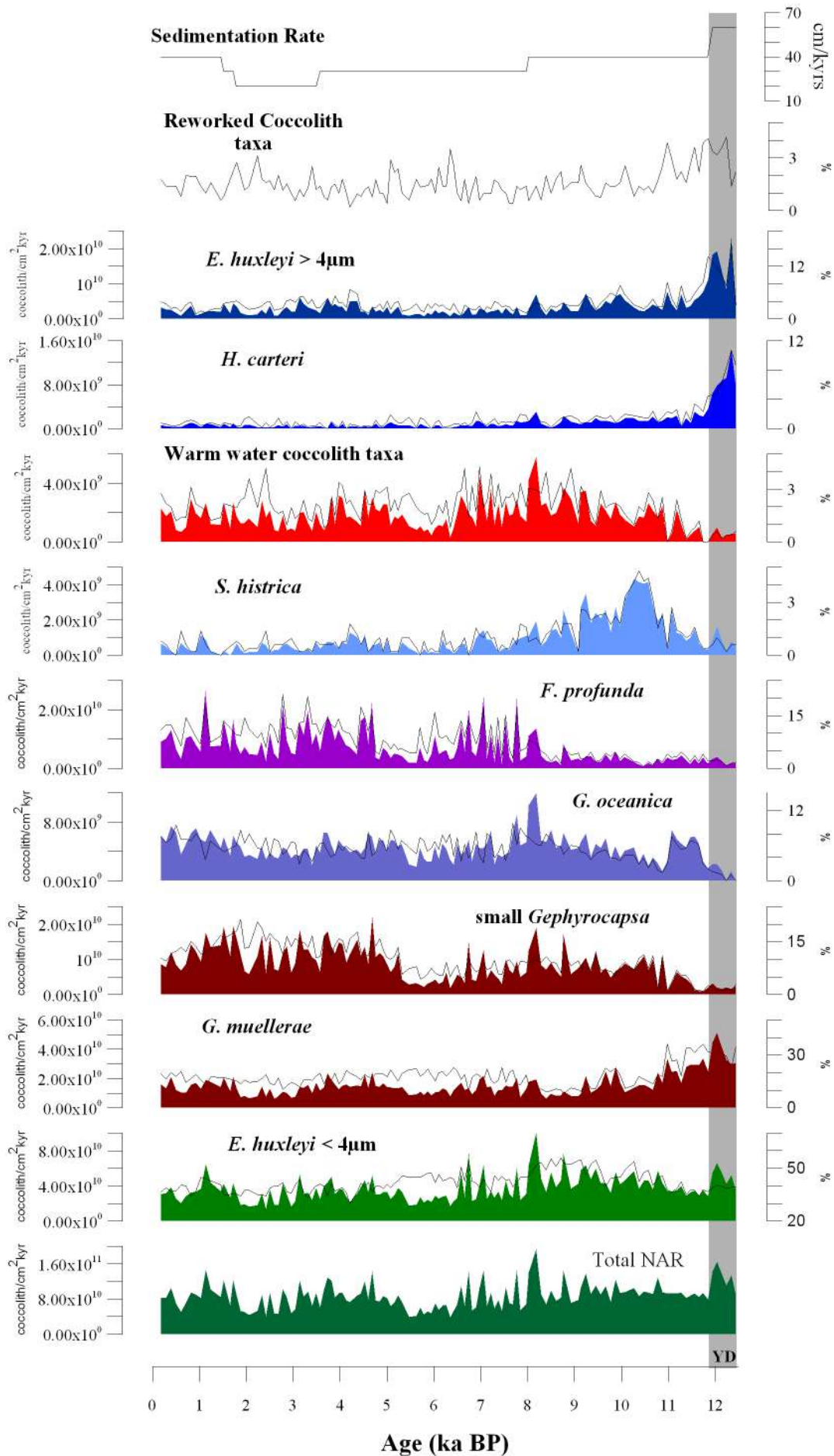
40  
41 1196

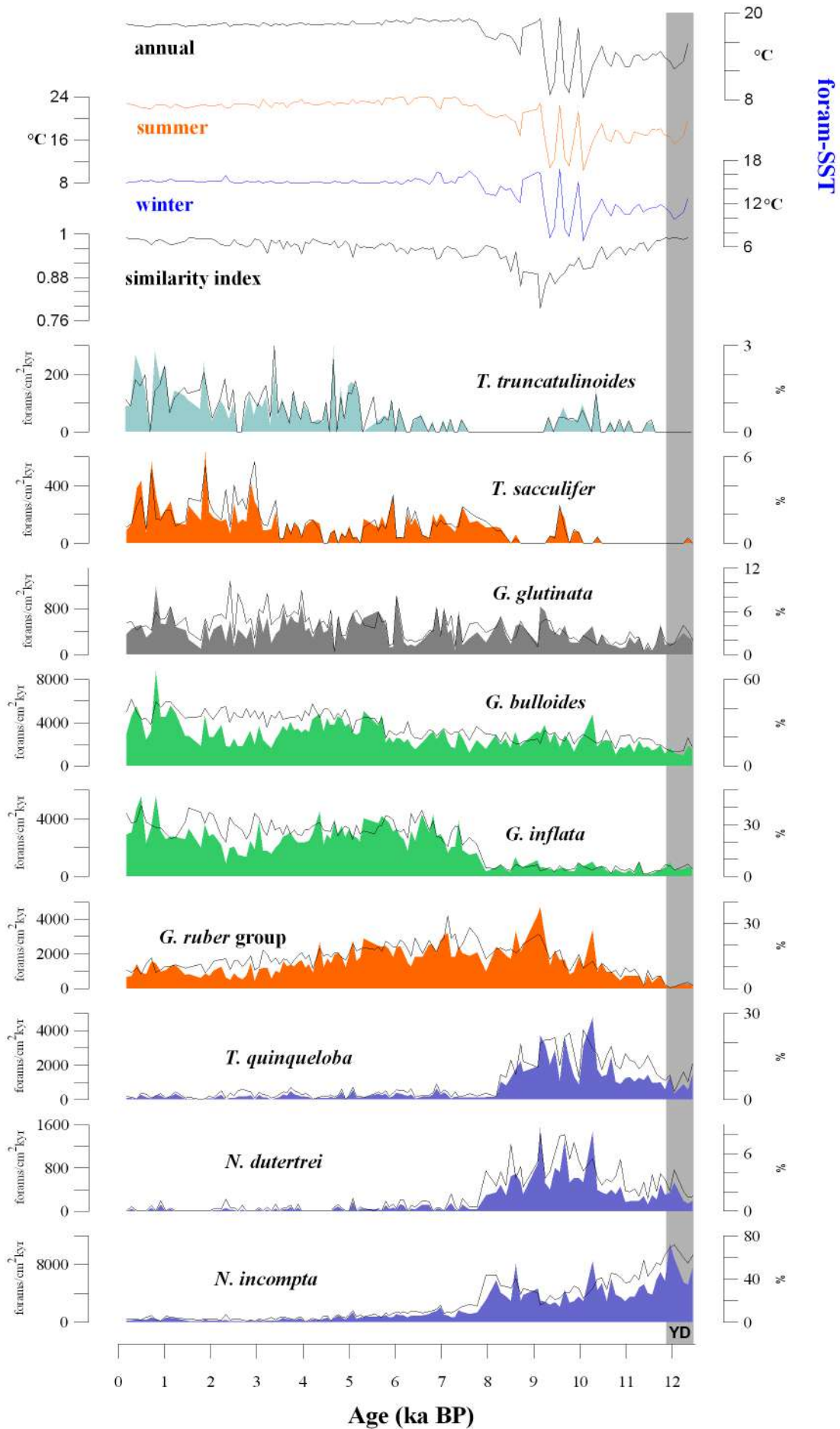
42  
43 1197

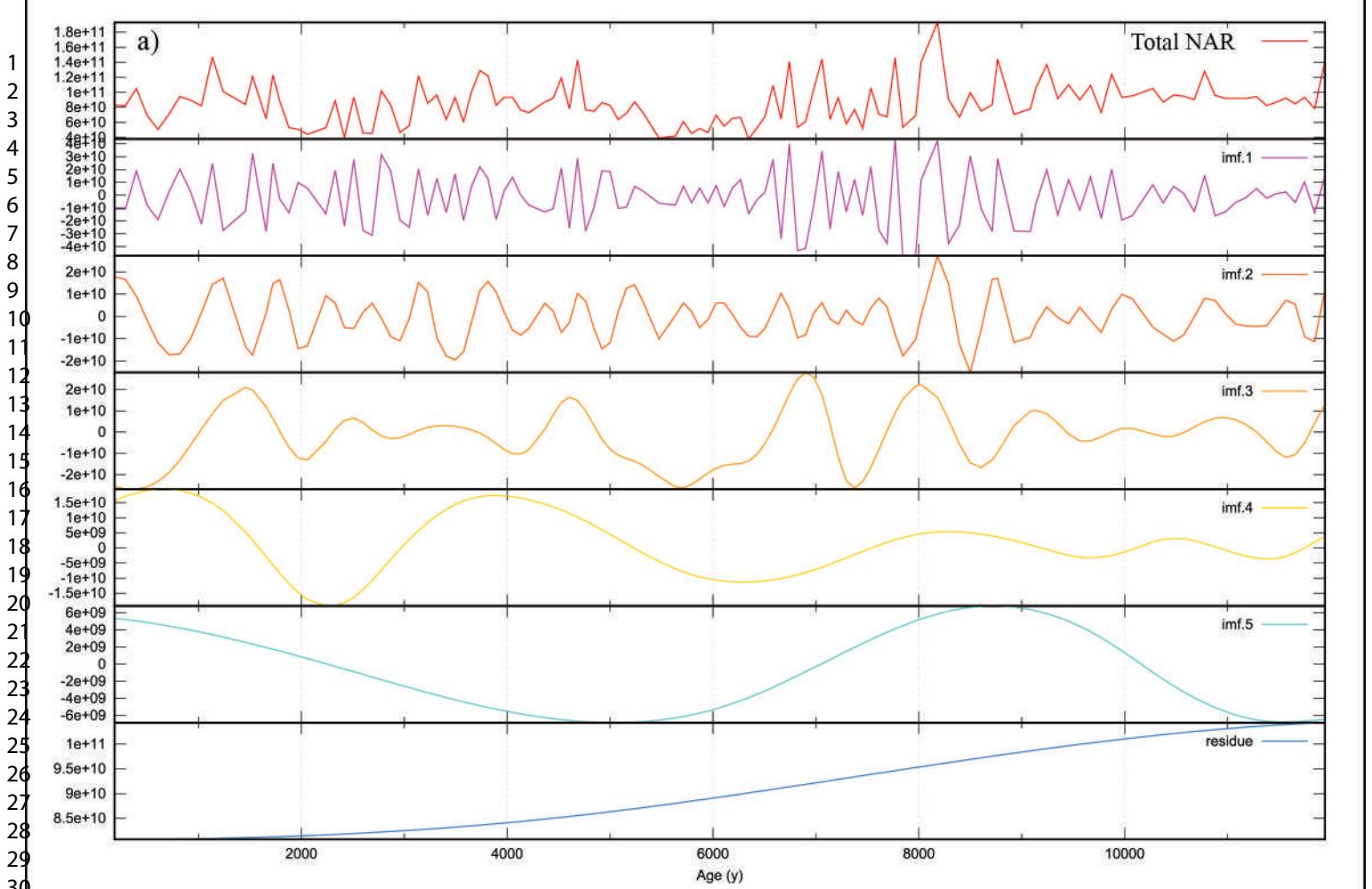
44 1198





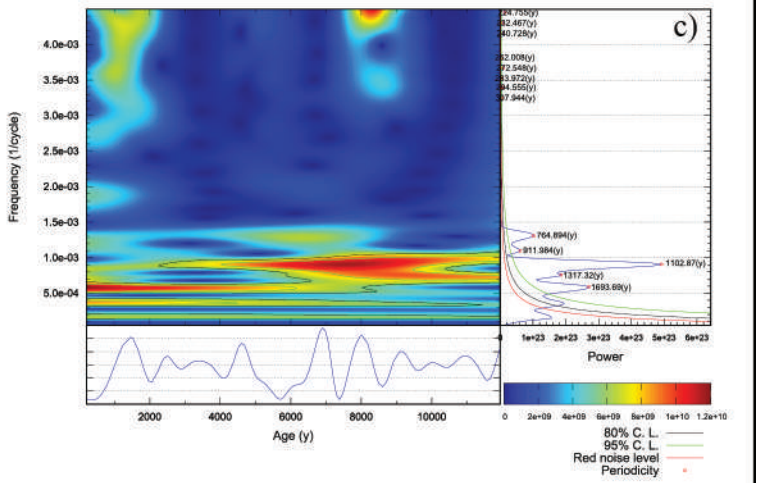
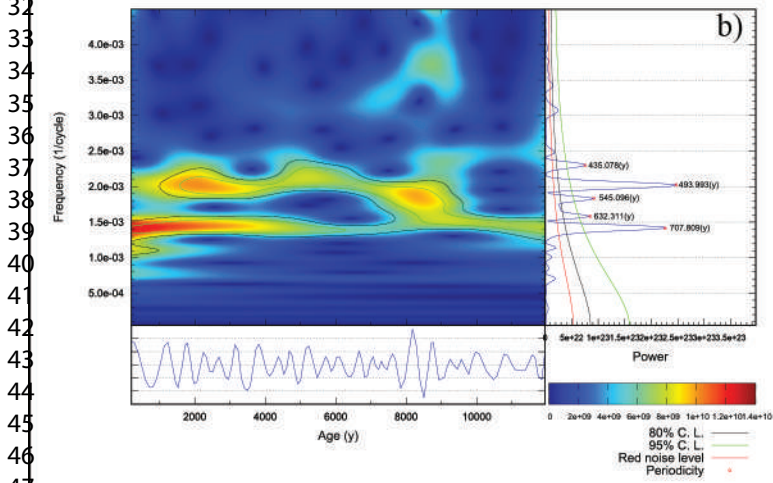






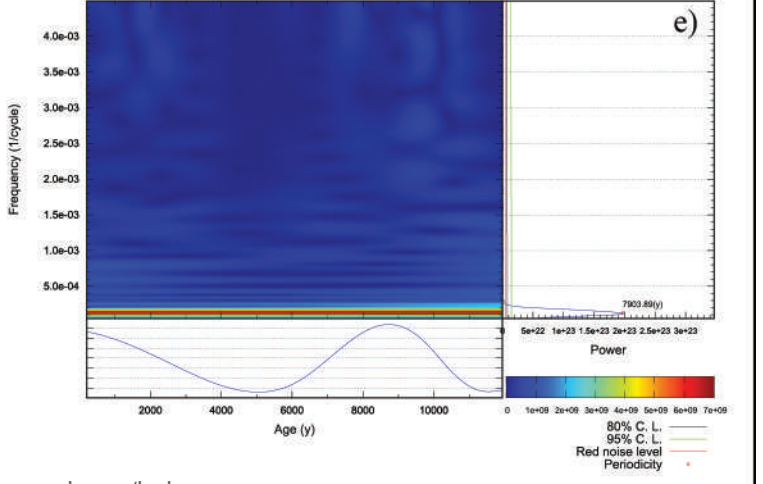
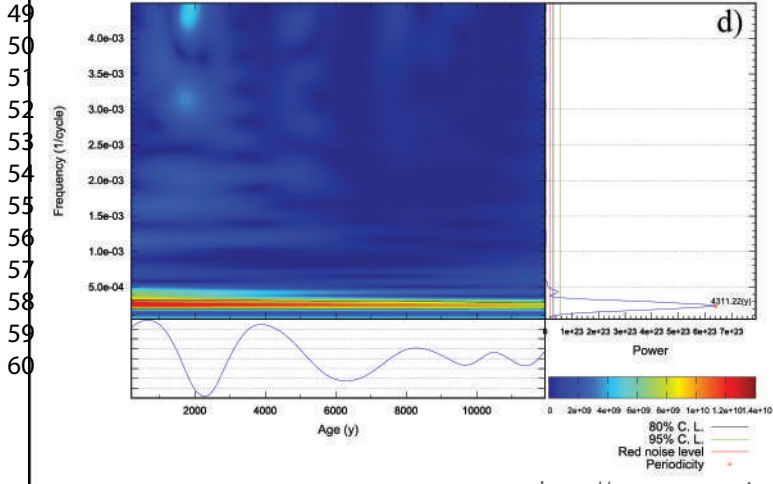
Total NAR IMF2

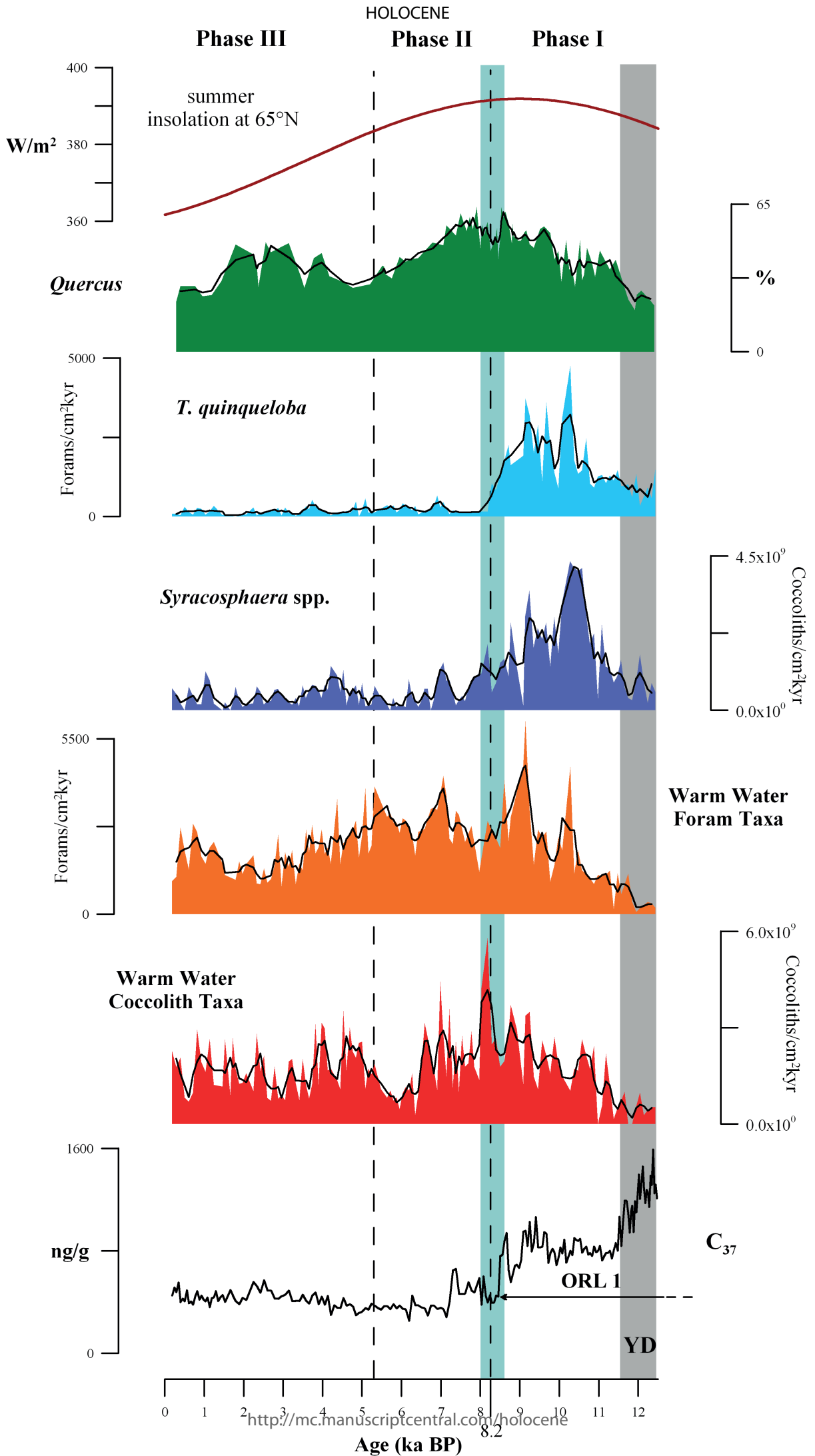
Total NAR IMF3



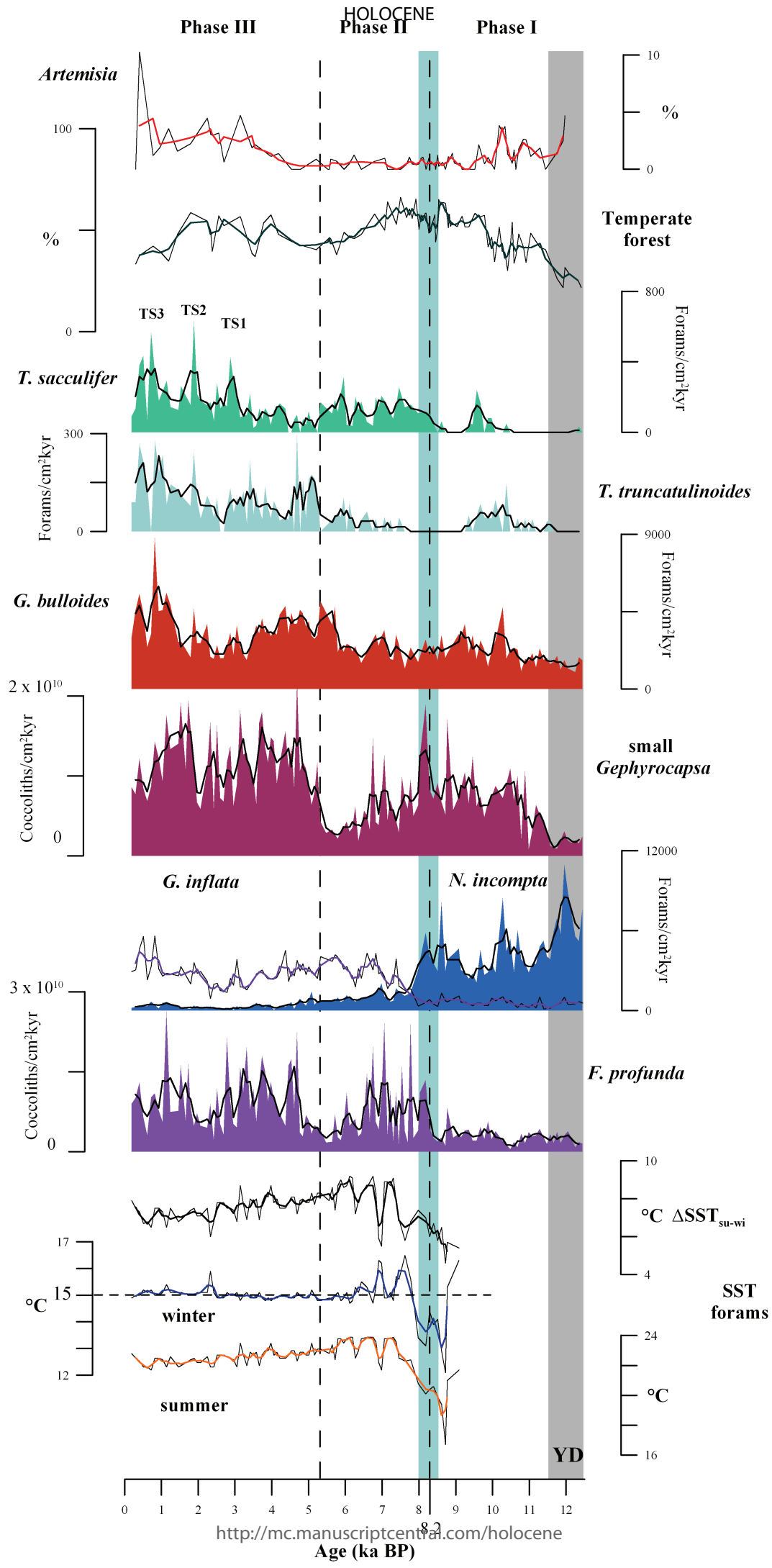
Total NAR IMF4

Total NAR IMF5

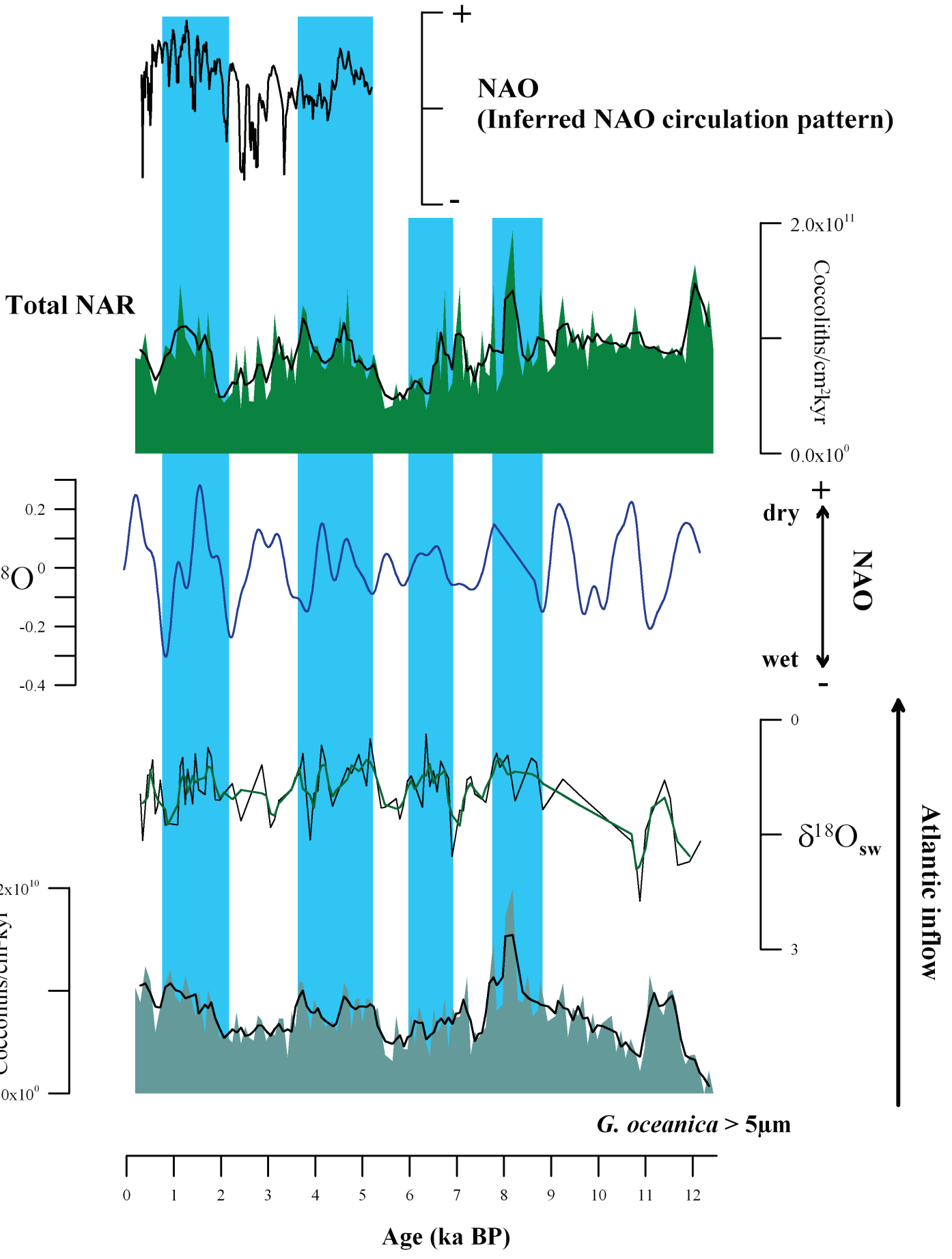




1  
2  
3  
4  
5  
6  
7  
8  
9  
10  
11  
12  
13  
14  
15  
16  
17  
18  
19  
20  
21  
22  
23  
24  
25  
26  
27  
28  
29  
30  
31  
32  
33  
34  
35  
36  
37  
38  
39  
40  
41  
42  
43  
44  
45  
46  
47  
48  
49  
50  
51  
52  
53  
54  
55  
56  
57  
58  
59  
60



1  
2  
3  
4  
5  
6  
7  
8  
9  
10  
11  
12  
13  
14  
15  
16  
17  
18  
19  
20  
21  
22  
23  
24  
25  
26  
27  
28  
29  
30  
31  
32  
33  
34  
35  
36  
37  
38  
39  
40  
41  
42  
43  
44  
45  
46  
47  
48  
49  
50  
51  
52  
53  
54  
55  
56  
57  
58  
59  
60



1  
2  
3  
4  
5  
6  
7  
8  
9  
10  
11  
12  
13  
14  
15  
16  
17  
18  
19  
20  
21  
22  
23  
24  
25  
26  
27  
28  
29  
30  
31  
32  
33  
34  
35  
36  
37  
38  
39  
40  
41  
42  
43  
44  
45  
46  
47  
48  
49  
50  
51  
52  
53  
54  
55  
56  
57  
58  
59  
60

